Investigation of the apoptotic pathway in glioblastoma in the context of suicide gene therapy

Gracious Takayidza

This thesis is submitted in partial fulfillment of the requirements for the degree of Master in Biomedical Sciences

Department of Biomedicine

University of Bergen

Spring 2023

Acknowledgements

I would like to thank everyone who in one way or the other contributed to the completion of this thesis. First and foremost, I am immensely thankful to my supervisor, Prof. Hrvoje Miletic for graciously accepting me to his group. He provided me with a tremendous opportunity to better my knowledge of translational cancer research. It is with his constant supervision and guidance that this work came into existence. I am also deeply thankful to my co-supervisors, Dr. Hossain and Ege Solel who have been extremely reliable sources of practical scientific knowledge. I gained a lot from their vast knowledge and scientific curiosity. They patiently introduced me to new analytical research techniques. I am grateful for their guidance, support, and comments throughout the work.

I owe a debt of gratitude to all our group members. I thank Shannon Moreino and Egil Brudvik who always had a mysterious way of showing up whenever I had questions, which I definitely knew they had answers to. Additionally, it has been a pleasure working with Lara Lommers, the random short talks and laughs we shared would somehow find a way to brighten the days. Special mention to Romi Roy Choudhury whom at some point, out of her tight schedules, wholeheartedly assisted me in learning new techniques. I would like to thank the technical staff, Halala Sdik Saed and Aurea Castilho who provided immediate support for any technical issues. They provided a friendly and cooperative atmosphere which made it so easy to approach them when in need of any assistance. I would be remiss if I did not mention Dr Tambudzai Jakobsen and Prof. Martha Enger, my mentors. These two have been my unending source of inspiration and encouragement. They constantly nurtured my determination and kept me mentally strong with their words of advice.

Finally, I would like to acknowledge my friends and family for their unwavering support. I would like to thank Brian and Tinashe for their love and support. I thank my loving husband Tich and patient son Adiel for being my constant pillars of unyielding support and strength. This thesis is heartily dedicated to my mom who always believed in me and taught me to believe in myself during her life on earth.

Contents

Abbreviations

AAV Adeno-associated virus

APAF-1 Apoptotic protease-activating factor 1

APCs Antigen presenting cells

APS Ammonium persulfate

ATM Ataxia Telangictasia Mutated

ATP Adenosine triphosphate

AV Adenovirus

BAK B-Cell Leukemia/Lymphoma 2 antagonist/killer

BAX B-Cell Leukemia/Lymphoma 2-associated X protein

BBB Blood brain barrier

BCA Bicinchoninic acid

BCL-2 B-Cell Leukemia/Lymphoma 2

BER Base-excision repair

BH B-Cell Leukemia/Lymphoma 2 homology

BID B-Cell Leukemia/Lymphoma 2 homology 3 Interacting domain death antagonist

BIM BCL-2 interacting mediator of cell death

BRAF B-type RAF proto-oncogene

BRCA1 Breast cancer gene 1

BSA Bovine serum albumin

Cas9 Clustered Regularly Interspaced Short Palindromic Repeats-associated protein 9

CD Cytosine deaminase

CDKN2A Cyclin dependent kinase inhibitor 2A

CHO Chinese hamster ovary

CNS Central nervous system

CRISPR Clustered Regularly Interspaced Short Palindromic Repeats

DAMPS Damage associated molecular patterns

DISC Death-inducing signaling complex

DMEM Dulbecco's Modified Eagle's Medium

DMSO Dimethyl sulfoxide

DNA Deoxyribonucleic acid

DPBS Dulbecco's phosphate buffered saline

DR Death receptor

DTT Dithiothreitol

EDTA Ethylenediamine tetraacetic acid

EGFR Epidermal growth factor receptor

FADD Fas-associated death domain

FastAP Fast alkaline phosphatase

FasL Fas ligand

FBS Fetal bovine serum

GBM Glioblastoma

GCV Ganciclovir

GeCKO Genome-scale Clustered Regularly Interspaced Short Palindromic Repeats Knock-out

GLOBOCAN Global Cancer Statistics

GSDME Gasdermin E

HBV Hepatitis B virus

HCV Hepatitis C virus

HMGB1 High mobility group box 1

HPV Human papilloma virus

HRP Horseradish peroxidase

hSpgene X Humanized *S.pyogenes* gene X

HSV Herpes simplex virus

IAP Inhibitors of apoptosis (IAP)

ICD Immunogenic cell death

IDH Isocitrate dehydrogenase

IL Interleukin

Indels Insertions or deletions

Kb Kilobase

KO Knock out

LB Luria Broth

LDH Lactate dehydrogenase

LDS Lithium dodecyl sulfate

Lvs Lentiviruses

MAP1LC3 Microtubule-associated protein 1A/1B-light chain 3

MCL1 Myeloid leukemia 1

MMR Mismatch repair

MOMP Mitochondrial outer membrane permeabilization

MYC Myelocytomatosis

NER Nucleotide-excision repair

NF1 Neurofibromatosis type 1

PAGE Polyacrylamide gel electrophoresis

PARP-1 Poly (ADP-ribose) polymerase-1

PCR Polymerase chain reaction

PDGFRA Platelet derived growth factor alpha

PFS Progression-free survival

PI Propidium Iodide

PTEN Phosphatase and tensin homolog

RAS Rat sarcoma

RB1 Retinoblastoma susceptibility

RNA Ribonucleic acid

ROS Reactive oxygen species

Rvs Retroviruses

SDS Sodium dodecyl sulfate

SGT Suicide gene therapy

Smac Second mitochondrial-derived activator of caspase

SOC Standards of care

SQSTM1 Sequestosome 1

tBID Truncated BH3 Interacting domain death antagonist

TEMED Tetramethylethylenediamine

TGF-β Transforming growth factor-beta

TK Thymidine kinase

TME Tumor microenvironment

TMZ Temozolomide

TNF Tumor necrosis factor

TNFR Tumor necrosis factor receptor

TP53 Tumor protein 53

TRADD Tumor necrosis factor receptor type1-associated death domain

TRAIL Tumor necrosis factor -related apoptosis inducing ligand

TTF Tumor-treating fields

U.S. FDA United States Food and Drug Administration

VEGF Vascular endothelial growth factor

WHO World health organization

WST Water soluble tetrazolium salt

XIAP X-linked inhibitors of apoptosis

5-FC 5-fluorocytosine

List of Figures

List of Tables

Summary

Glioblastoma is a highly malignant, aggressive and most common primary brain tumor in adults. Tremendous research efforts have been conducted in the field of GBM treatment discovery and succcess has only been achieved at pre-clinical level. Despite numerous approaches used in the treatment of GBM, patients still experience tumor progression, show extremely poor prognosis, high mortality and barely 12-15 months of median survival. To a certain extent, the failure of current treatment modalities to provide durable responses is due to tumor heterogeneity, a hostile tumor microenvironment and the tumor's unique ability to evade the host's immune system.

Suicide gene therapy strategies are among the ongoing clinical studies for the treatment of GBM. Previous work from our lab shows that treatment of CT2A and GL261 mouse glioma cell lines with HSV-TK GCV SGT induced the apoptotic mechanism of cell death. Apoptosis is known to be non-immunogenic, hence it does not stimulate antitumor immune responses. Therefore, in this study we aimed to block the apoptotic pathway and study potential activation of alternative cell death pathways following HSV-TK/GCV induced SGT, which could be more immunogenic. To achieve our aims, we blocked the apoptotic pathway by knocking out two crucial genes in the apoptotic pathway (gene x and y; due to patenting conflicts, the names are not revealed) by CRISPR/Cas9 technology. Thereafter, investigations were conducted to study potential activation of lytic mode(s) of cell death, which are known to be more immunogenic.

Our results demonstrate that CRISPR/Cas9 effectively knocks out our genes of interest. Due to limited time, further studies could not be conducted using gene y KO cells. Further experiments conducted using gene x KO cells reveal effective inhibition of the apoptotic pathway with delay in cell death in both cell models. We found that apoptosis was not the dominant mode of cell death in both KO cell lines and, no enhanced lytic cell death was observed in both KO cell lines. However, in GL261 KO cells, our findings suggested possible activation of another mode of cell death which needs to be categorized in the future. We recommend further investigations to be conducted to understand mechanisms involved in this mode of cell death.

Chapter 1

1 Introduction

1.1 Cancer

Cancer can be defined as a group of some of the worldwide most frequently diagnosed, biologically aggressive and fatal pathophysiological conditions. It has undergone intense research and yet there still is a huge knowledge gap in fully understanding their complex cellular and molecular pathology [1]. Taking into consideration the revolution in cancer research, cancer can be described as a genetic disease. Daniel M. Hausman interestingly defined cancer as "a puzzling and frightening disease or set of diseases" [2]. In 2018, the Global Cancer Statistics (GLOBOCAN) estimates indicated anticipation of 18.1 million new cancer cases and 9.6 million cancer deaths in 2018 for 36 cancers in 185 countries [3]. In 2020, GLOBOCAN provided an update on estimates of cancer incidence and mortality, stating that worldwide, 19.3 million new cases and almost 10 million cancer deaths occurred in 2020 [4]. The study was conducted for 36 cancers in 185 countries as well, which indicates that overall, the burden of cancer incidence and mortality is on the rise worldwide.

Cancer initiation and progression is dependent upon the acquisition of multiple driver mutations which in turn can yield three outcomes. Firstly, they can render oncogenes constitutively active or activate in conditions under which the wild type would be inactive. Such mutations can arise due to gene amplifications, chromosomal translocations or subtle intragenic mutations that affect crucial residues involved in the regulation of gene product activities. Rat sarcoma (RAS), a group of frequently mutated genes in human cancers that is found to be mutated in 19% of cancer patients [5], Myelocytomatosis (MYC) genes that are frequently upregulated in primary brain cancers [6, 7] and the B-type RAF proto-oncogene (BRAF) that is mutated in most human cancers [8] are some examples of oncogenes.

Secondly, driver mutations can inactivate tumor suppressor genes through epigenetic silencing, missense mutations at residues that are crucial for gene activity and deletions or insertions (indels) of various sizes [9]. Tumor protein 53 (TP53), the guardian of genome, has been described as the most important tumor suppressor gene as it is most frequently mutated in human cancers [10]. The retinoblastoma susceptibility (RB1) gene, is another example of a tumor suppressor gene that is mutated in almost all familial and sporadic cases of retinoblastoma and, it is the first tumor suppressor gene that was molecularly defined [11]. Mutations in oncogenes and tumor-suppressor genes have a similar effect at physiologic level. They facilitate the neoplastic process by raising the number of tumor cells and this happens either through stimulation of cell division or inhibition of apoptosis or cell-cycle arrest [9].

The third possible outcome is that the stability genes, also known as deoxyribonucleic acid (DNA) repair genes, can be mutated, and they facilitate tumorigenesis in a different way from oncogenes and tumor suppressor genes. Stability genes are responsible for the repair of errors that occur during normal DNA replication or errors that are due to mutagen exposure, for example, mismatch repair (MMR), base-excision repair (BER), and nucleotide-excision repair (NER) genes [9]. Other stability genes, for instance breast cancer gene 1 (BRCA1) and Ataxia Telangictasia Mutated (ATM) genes which are most frequently mutated in breast cancer patients [9, 12], are responsible for mitotic recombination and chromosomal segregation, and these processes involve a large portion of chromosomes. The role of stability genes is to keep genetic mutations to a minimum and therefore, their inactivation translates to a higher mutation rate of the other genes [13]. If the mutated genes are oncogenes and tumor suppressor genes, the result is a dysregulated net cell growth which confers a selective growth advantage to the mutant cells which in turn, initiates tumorigenesis [9].

Several reports from etiological studies conducted on cancer support that cancer causal agents are heterogenous, ranging from genetic mutations (some of which have been discussed above), epigenetic to non-genetic causes including viral infections (hepatitis B virus (HBV), hepatitis C virus (HCV), retroviruses (Rvs) and human papilloma virus (HPV)) [14], bacterial and parasitic agents (H. pylori and S. Haematobium) [15], exogenous risk factors and/or lifestyle [16] and so on.

Cancers can both undermine and exploit mechanisms of multicellular organization. The diverse biological processes that occur in normal cells which lead to cancer were simplified by Hanahan and Weinberg in their first introduction of the six hallmarks of cancer in 2000. They explained that cancer cells: (i) are self-sufficient in growth signals, (ii) have reduced sensitivity for anti-growth signals, (iii) evade apoptosis, (iv) exhibit a limitless replicative potential, (v) develop the ability to sustain angiogenesis and (vi) invade and metastasize to other tissues [17]. A decade later they introduced reprogramming of energy metabolism and evasion of immune destruction as emerging hallmarks of cancer and pointed out genomic instability and inflammation as enabling characteristics of cancer hallmarks [18]. Recently, in 2022 Hanahan presented new prospective hallmarks and enabling characteristics that are namely; unlocking phenotypic plasticity, non-mutational epigenetic reprogramming, polymorphic microbiomes and senescent cells which might be incorporated as core components of hallmarks of cancer in the future [19]. The validated and proposed hallmarks of cancer and its enabling characteristics are summarized as illustrated in Figure 1.1.

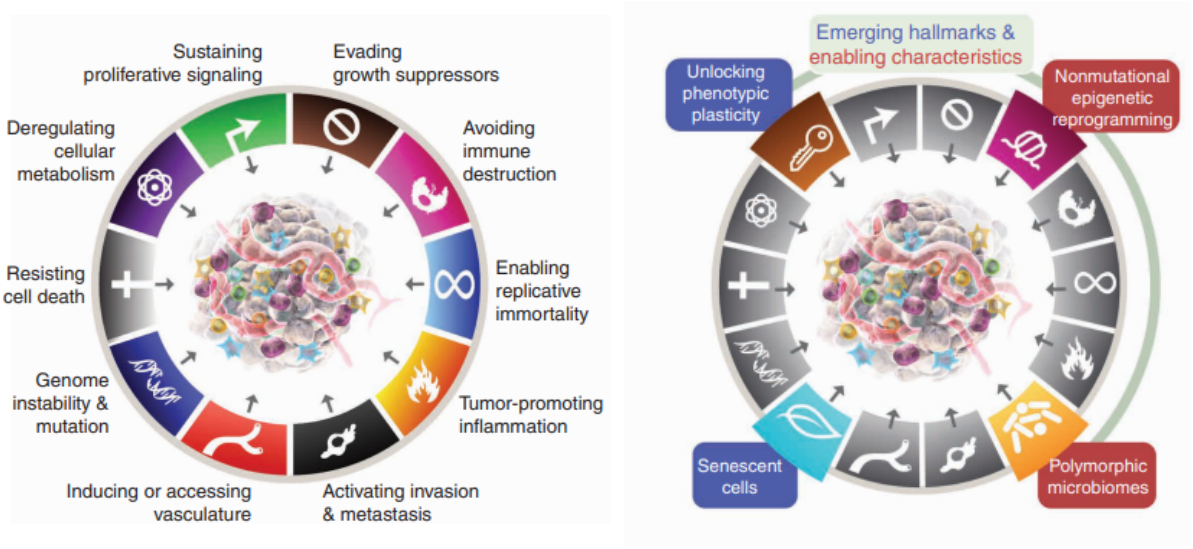

(a) (b)

Figure 1.1: Hallmarks and enabling characteristics of cancer. (a) The eight hallmark capabilities essential for the growth and progression of cancer and two enabling characteristics of cellular transformation and (b) the recently proposed two emerging cancer hallmarks and two cancer enabling characteristics. The graphic illustrations are adapted from [19] and [18].

1.2 Brain tumors

Brain tumors are common in the general population, however, occur less frequently compared to other cancers. While some brain tumors can be asymptomatic and found incidentally, others present with clinical symptoms such as focal neurological symptoms, headaches and seizures [20]. Intracranial metastasis from systemic cancers, meningiomas and gliomas are amongst the most prevalent types of brain cancers [20]. Lung cancers, breast cancers and melanomas often metastasize to the brain [21]. Brain metastases are more common than primary brain tumors with an incidence that is approximately 10 times more than that of primary brain tumors [22]. Various metastatic tumors can be controlled by therapy for months or years but, however, this is not the case with brain metastases. Regardless of how vigorous the treatment can be, survival remains inevitably short with median survival of months and 2-year survival of approximately 6% [23]. Neurosurgery, radiation, and chemotherapy are the standard of care treatment modalities for brain tumors. Meningiomas are mostly benign, slow growing and the most common primary brain tumor. Glioma refers to a group of primary malignant tumors of the central nervous system (CNS) [20] which include astrocytomas, ependymomas and oligodendrogliomas [24].

1.3 Glioblastoma (GBM)

GBM is defined as world health organization (WHO) grade 4 glioma of the CNS [25]. It is the most aggressive and common malignant primary brain and other CNS tumor in adults, with an extremely poor prognosis [26]. As shown in (Figure 1.2), GBM constitutes 14.3% of all primary brain and other CNS tumors and nearly half of all malignant tumors within the brain and CNS [26, 27].

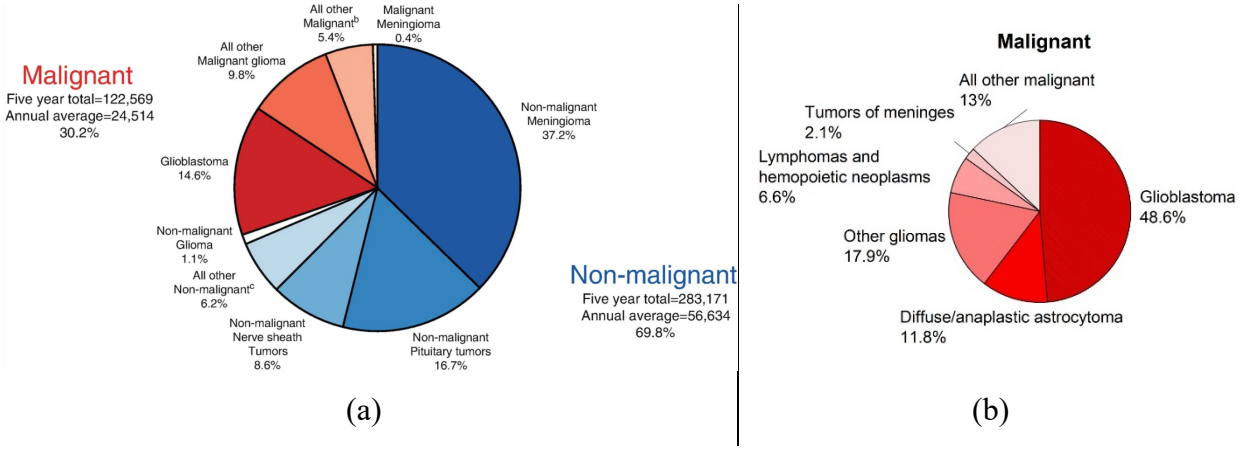

Figure 1.2: Distribution of primary brain and other CNS tumors by behavior in the USA (2014-2018). Distribution of malignant Brain and other Central Nervous System Tumors by behavior and major histology type in USA (2013-2017). Figures extracted from [26, 27].

1.3.1 Classification of GBM

Classification of GBM uses both histological features and molecular parameters. GBM can be of primary or secondary origin whereby; primary GBMs develop rapidly *de novo* in older patients (>50) with no clinical or histologic evidence of a less malignant precursor lesion. Secondary GBMs, on the other hand, originate and progress from either low-grade diffuse astrocytomas or anaplastic astrocytomas, and they manifest in younger patients. Due to the different origins of secondary GBM, its name has been changed to astrocytoma (WHO grade 4) in the new WHO classification [28]. Primary GBM and astrocytoma (WHO grade 4) differ in their genetic and epigenetic profiles but histologically, they are largely indistinguishable. Primary GBMs carry a worse prognosis in comparison to secondary GBMs [29].

The latest WHO classification subdivides GBM and astrocytomas according to their isocitrate dehydrogenase (IDH) mutational status into (1) IDH-wildtype GBM which constitutes approximately 90% of cases, and (2) IDH-mutant astrocytoma which is the remaining approximately 10% of cases [29]. Depending on their unique molecular signatures, GBMs can be further classified into classical, proneural and mesenchymal subtypes [30, 31]. Classical subtype is characterized by epidermal growth factor receptor (EGFR) amplification, a lack of TP53 mutations and homozygous deletion of cyclin dependent kinase inhibitor 2A (CDKN2A). Proneural tumors are characterized by platelet derived growth factor alpha (PDGFRA) expression

and have the best prognosis. Mesenchymal tumors are characterized by neurofibromatosis type 1 (NF1) expression which is often co-mutated with phosphatase and tensin homolog (PTEN) and they have the worst prognosis [30, 31]. GBM has a highly heterogenous tumor microenvironment (TME), a single GBM tumor can have multiple subtypes at different regions [32, 33].

1.3.2 GBM treatment modalities

The current standards of care (SOC) treatment of GBM comprise of gross total resection of the tumor tissue and follow up adjuvant treatment with radiation therapy and chemotherapy with temozolomide (TMZ), an oral alkylating agent that was introduced in 2005 [34, 35]. Patients with recurrent GBM can be further treated with bevacizumab, a humanized monoclonal antibody against the vascular endothelial growth factor (VEGF) which was approved in 2009 by the United States Food and Drug Administration (U.S. FDA) [36]. Several studies have clearly shown that the use of either both bevacizumab and chemotherapy or bevacizumab alone in recurrent GBM patients yields radiographic responses and increases progression-free survival (PFS) in comparison to data from patients receiving chemotherapy alone [36]. However, some studies have revealed that bevacizumab fails to prolong overall survival [37]. Despite substantial therapeutic efforts invested in the field of anti-GBM drug-discovery in the past decade, and various combinatorial treatment regimens designed against GBM, GBM patients still show an extremely poor prognosis with a median of survival of only 12-15 months [38] and 5 year survival rate of 6.8% [39]. Patients with recurrent GBM have an even more dismal prognosis with just 25 - 40 weeks median of survival [40].

The blood brain barrier (BBB) is one of the major challenges faced with regards to GBM treatment. Further obstacles are intra and inter-tumoral heterogeneity, an inherent immunosuppressive microenvironment and tumor plasticity which all remain as barriers that are yet to be overcome [41]. Endothelial, immune, and other parenchymal cells make up the GBM TME and these cells promote angiogenesis, invasion, proliferation, and they also facilitate immune suppressive functions [41, 42]. GBM has a substantial immune compartment, consisting mainly of cells originating from the myeloid lineage but despite that, GBMs are quite efficient at evading the host immune surveillance [43]. Immunotherapeutic treatments therefore seek to redirect the patient's

immune cells against the tumor. However, clinical trials using checkpoint inhibitors showed disappointing results without effect on overall survival [44, 45]. Out of the multitude of clinical trials that have been conducted in the last decade, one of the few that has been moderately successful in improving overall survival is the tumor-treating fields (TTF) device used for recurrent or refractory GBMs [46]. It was approved in 2011 by the U.S FDA. TTF used in combination with chemotherapy increased overall survival to 20.9 months in comparison to 16 months survival seen in patients treated with chemotherapy alone in a phase III clinical trial involving newly diagnosed GBM patients [46]. The failure of past therapeutic measures aimed to improve the current GBM SOC to some extent reflect the rapid and aggressive nature of GBM progression. Therefore, there is desperate need to identify novel therapeutic strategies of complementing SOC.

1.4 Gene therapy and Suicide gene therapy (SGT)

1.4.1 Gene therapy

Gene therapy can be defined as the introduction of genetic materials into human cells for therapeutic purposes. Cancer gene therapies generally alter the genetic makeup of tumor cells thereby effecting various changes in cancer cells which can result in their direct cytotoxicity, interference with tumor resistance pathways or modifications in the microenvironment and so on. Viral or non-viral vectors are used to successfully deliver therapeutic genes to brain cancer cells. Viral vectors are considered to be the most effective gene delivery method for in vivo gene transfer [47, 48]. Anti-glioma therapy utilizes either replication deficient viruses that can transduce suicidal genes into tumor cells or replicating oncolytic viruses with a lytic cycle that preferentially kill tumor cells. All gene therapy approaches face a common challenge of efficacy, and this is especially more pronounced in GBM due to its highly invasive and diffuse nature in comparison to other tumor types [49].

1.4.2 Suicide gene therapy

In SGT, tumor cells are transduced with the so-called suicide gene. The suicide gene induces the expression of an enzyme (that is absent or expressed at low levels in mammalian cells) that can

catalyze the non-toxic prodrug, which is administered externally, to produce a cytotoxic metabolite that induces tumor cell death. The herpes simplex virus-thymidine kinase/Ganciclovir (HSV-TK/GCV) and cytosine deaminase (CD)/5-fluorocytosine (5-FC) systems are the two well studied suicide gene therapy approaches [50]. The HSV-TK gene, coupled with systemic administration of GCV as a prodrug system was first reported in 1986 by Moolten [51]. In this model, cancer cells are transduced with the HSV-TK gene followed by systemic administration of GCV. HSV-TK then firstly, monophosphorylates the nucleoside analogue of GCV. The monophosphorylated GCV is then further converted to triphosphate GCV within the host cells. Following that, triphosphate GCV is incorporated into the DNA thereby blocking DNA replication and inhibiting cell division and inducing apoptosis [50]. The resulting phosphorylated nucleoside analogues spread through gap-junctions leave to the surrounding cells thereby effecting the bystander effect [52]. The suicide gene therapy strategy is illustrated in Figure 1.3. In previously conducted large clinical trials, suicide gene therapy has failed to show therapeutic benefits [53], hence the need for suicide gene therapy improvement.

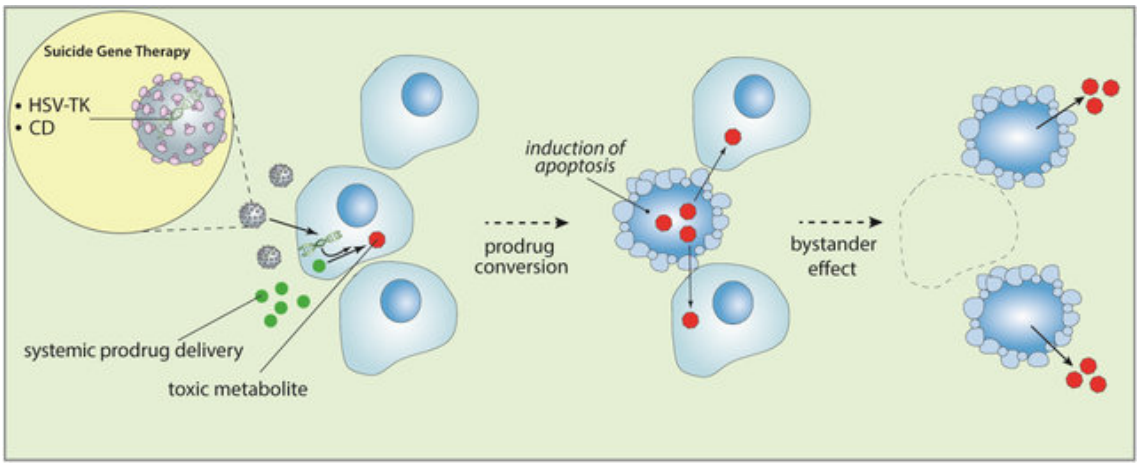

Figure 1.3: Suicide gene therapy strategy. A nontoxic prodrug is systematically administered. Thereafter, a gene encoding for an enzyme that catalyzes the pro-drug into a toxic metabolite is delivered to tumor cells through a tumor-targeting viral vector. The resulting toxic metabolites induce cell death in transduced cells and the non-transduced cells at tumor site also undergo cell death due to by-stander effect. Figure extracted from [54]

1.4.3 Gene therapy delivery methods

Suicide gene therapy can only be as efficient as its ability to deliver the suicide genes in clinical settings [55]. Suicide gene therapy has so far employed several viral vectors to directly deliver therapeutic genes into tumor sites such as adenovirus (AV), herpes simplex virus (HSV), retroviruses, adeno-associated virus (AAV) and lentiviruses (LVs) [48, 56, 57]. Herpes Simplex Virus-1 (HSV-1) is widely used in CNS gene therapy and GBM gene therapy because of its neurotropism, capability to package large therapeutic genes (~160 Kb of DNA) and its long-lasting gene expression in neurons [58]. However, LVs have gained so much attention of late due to their crucial ability to integrate into the genome of both dividing and non-dividing cells [59].

1.5 Apoptosis

Apoptosis, initially known as the concept of cell death is possibly one of the ancient ideas in cell biology [60]. Apoptosis is a tightly regulated multi-step pathway that facilitates tolerogenic cell death during development and in adult multicellular organisms [61]. It has a crucial role in the control of cell numbers and in physiological and pathological conditions [62]. Physiological apoptotic signaling is of vital importance in the maintenance of a healthy balance between cell survival and cell death and in safeguarding the genome integrity as seen in the establishment of the evasion of apoptosis as one of the major cancer hallmarks [18]. In 1972, Wyllie and Currie first brought up the idea that tumor development and progression could be influenced by apoptosis upon observing that tumor growth rate was less than predicted due to high level of endogenous tumor cell apoptosis [63]. Dysregulations in the apoptotic signaling pathway also equips tumor cells with resistance to conventional methods of treatment such as chemotherapy and radiotherapy as these treatment modalities exert their antitumor effects mainly through the induction of apoptosis in cancer cells [64]. Apoptotic cell death is regulated by two major signaling pathways, the intrinsic (or mitochondria-dependent) and extrinsic (or death-receptor mediated) pathway which both activate caspases as effector mechanism of apoptosis [65] as summarized in Figure 1.4**.**

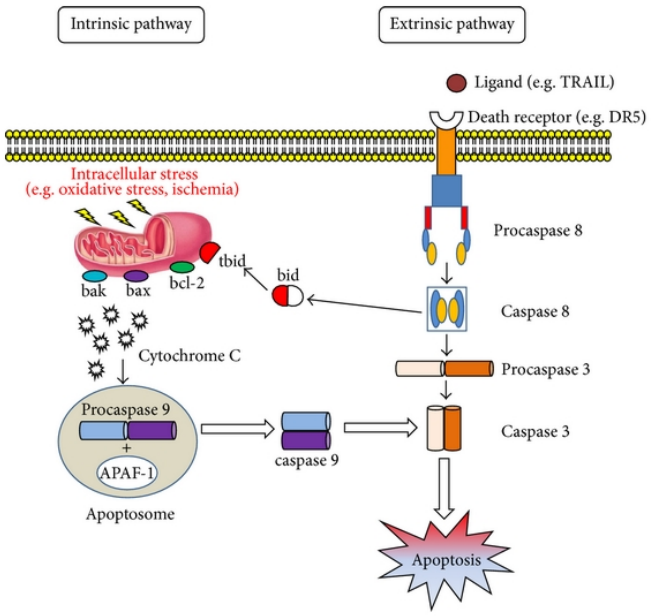

Figure 1.4: Apoptotic pathways summary, figure extracted from [66]

Caspases are a group of cysteine proteases found in the cytosol in an inactive form. During apoptosis, they are proteolytically cleaved at specific aspartate residues thereby becoming activated [67]. Most of the morphological changes which characterize apoptotic cell death are caused by caspases through their cleavage of different substrates in the nucleus or cytoplasm [68]. Hence the referral to caspases as the central executioners of the apoptotic pathway. Elimination of caspases through any means will either slow down or inhibit apoptosis [69]. Caspase-3, and -7 are the downstream activator caspases also referred to as the workhorses of the caspase family and they are activated through the caspase cascade. The caspase cascade illustrating the activation of caspases leading to apoptosis is shown in Figure 1.5.

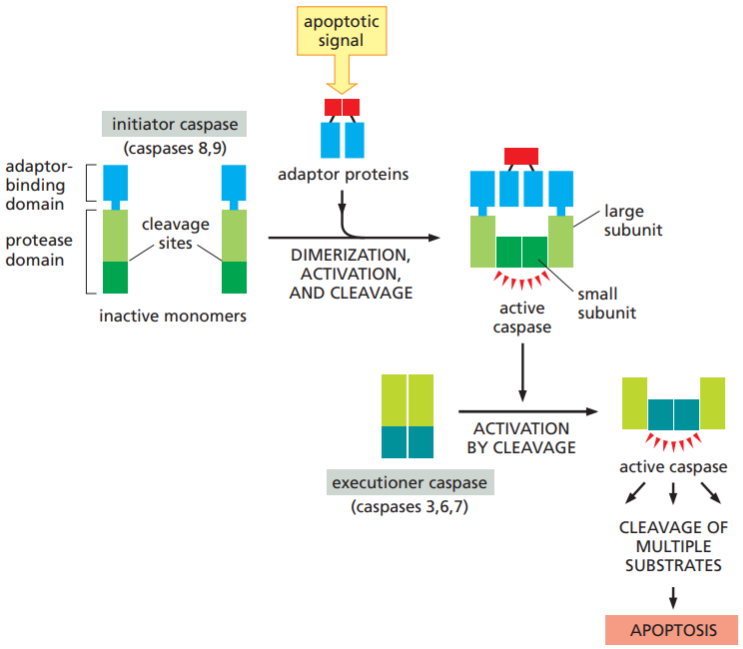

Figure 1.5: Summary of the caspase cascade, figure extracted from [70]

1.5.1 Extrinsic pathway

In the extrinsic pathway, death receptors present on cell membranes, such as CD95 (or Fas), death receptor 4 (DR4) and death receptor 5 (DR5) bind to their respective death receptor ligands which are soluble or transmembrane proteins for instance Fas ligand (FasL) and tumour necrosis factor (TNF)-related apoptosis inducing ligand (TRAIL) [71]. Following their binding, the death receptors further go on to oligomerize and recruit procaspase 8 and adaptor proteins such as TNF receptor (TNFR) type1-associated death domain (TRADD) or Fas-associated death domain (FADD) resulting in formation of the death-inducing signaling complex (DISC). Within the DISC, procaspase 8 is auto-proteolytically cleaved and thereby activated in this process into caspase-8 (the key initiator caspase in the extrinsic pathway). Caspase-8 can either directly induce apoptosis by activating caspase-3 (an executioner caspase) or indirectly by proteolytically converting BH3 Interacting domain death antagonist (BID) to its truncated form, tBID. The tBID then associates with the mitochondrial outer membrane and/or promotes Bax activation and oligomerization, resulting in apoptosis induction through the intrinsic pathway [66, 72].

1.5.2 Intrinsic pathway

The intrinsic pathway is triggered by upstream cellular stress signals such as DNA damage, reactive oxygen species (ROS) and growth factor deprivation. These induce mitochondrial outer membrane permeabilization (MOMP) which in turn leads to the release of cytochrome c or second mitochondrial-derived activator of caspase (Smac) (alternatively called DIABLO) from the mitochondrial membrane space into the cytosol [73]. Cytochrome c activates apoptotic protease-activating factor 1 (Apaf-1), which oligomerizes to form a caspase-activating complex referred to as the Apaf-1 apoptosome [74]. Caspase-9 (an initiator caspase), unlike other caspases has a complex activation mechanism. Proteolytic cleavage of procaspase-9 is not sufficient for the activation of caspase-9 catalytic activity [75]. It is required that caspase-9 associates with Apaf-1, and cytochrome c for its activation. The resulting Apaf-1/caspase-9 holoenzyme complex is thought to be the active form of caspase-9 [76]. Apaf-1 is therefore not just a caspase activator but rather an essential regulatory subunit of a caspase-9 holoenzyme frequently referred to as an apoptosome [74]. The apoptosome subsequently recruits the effector caspase-3 through interactions between caspase-9 active site cysteine and caspase-3 aspartate cleavage sites resulting in the cleavage of caspase-3 into its activate form. This marks the initiation of the caspase cascade which executes apoptosis. Activated caspase-3 cleaves poly(ADP-ribose) polymerase-1 (PARP-1) (that has a primary function in the detection and repair of DNA damage), and PARP-1 cleavage is known to promote apoptotic cell death [77].

Various proteins are involved in the regulation of apoptosis. (B-Cell Leukemia/Lymphoma 2) BCL-2 family proteins discussed below tightly regulate the process of MOMP. Whilst cytochrome c initiates apoptosis by activation of effector caspase-3, Smac facilitates apoptosis by antagonizing inhibitors of apoptosis (IAP) proteins for example x-linked IAP (XIAP), thus freeing caspases to activate apoptosis. XIAP inhibits apoptosis by binding to caspases-3, 7 and 9 and inhibiting their activation [78]. Involvement of the intrinsic pathway is necessary in GBM cells in order to obtain full activation of downstream effector mechanisms through the amplification of the apoptotic signal [79]. MOMP is considered as the point of no return, thus once initiated, the cell will undergo death [80].

1.5.3 BCL-2 family

BCL-2 family consists of two types of proteins namely proapoptotic proteins and antiapoptotic proteins summarized in Figure 1.6.

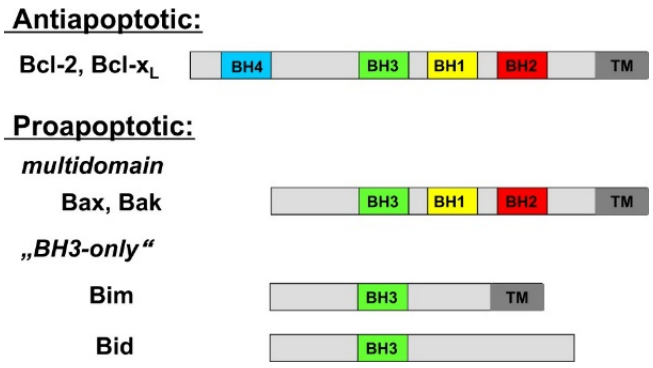

Figure 1.6: The BCL-2 family proteins, extracted from [81]

The antiapoptotic sub-family includes BCL-2, BCL-X_L, and myeloid leukemia 1 (MCL-1), which all contain three or four BCL-2 homology (BH) domains. The BH domain is required for the anti-apoptotic function of this BCL-2 protein family. They initiate interactions with other BCL-2 specifically at the mitochondrial level, where they regulate the release of pro-apoptotic mediators such as Smac [82]. The proapoptotic subfamily comprises of two sub-groups, (i)multi-domain proteins BCL2 antagonist/killer (BAK) and BCL-2 associated X protein (BAX), and (ii) BCL-2-homology domain -3 (BH3)- only proteins for example BCL-2 interacting mediator of cell death (BIM), Bid and NOXA that have a single BH3 domain [83]. These proapoptotic proteins function by forming pores or interacting with pore forming proteins at mitochondrial membrane level and BCL-2 protein is antagonistic to this function [60]. It has been seen that in malignant gliomas the antiapoptotic BCL-2 proteins are highly expressed [84]. In one report, high expression levels of BCL- X_L has been associated with poor progression and survival of GBM patients [85].

1.6 Immunogenic cell death (ICD)

ICD is a regulated form of cell death that can stimulate the adaptive immune responses. In recent decades it has been seen that ICD establishes relevant dialogue between dying cancer cells and the immune system following cancer therapy [86]. Cancer cell death induced by for instance, reactive oxygen species, and endothelium reticulum stress activates danger signals [87, 88]. The danger

signals will lead to the emission of damage associated molecular patterns (DAMPs) by dying cancer cells [89]. DAMPs are molecules that perform two different functions depending on their location. Intracellularly, DAMPs perform physiological functions and extracellularly, they stimulate inflammatory responses by alerting the body about danger. High mobility group box 1 (HMGB1) and adenosine triphosphate (ATP) are exemplary DAMPs that contribute to both tissue repair and inflammation [77]. These immunomodulatory molecules are recognized by pattern recognition receptors on the surfaces of antigen presenting cells (APCs) and propagate chemotaxis and maturation of the APCs. These processes in conjunction with uptake of tumor antigens from the dead and dying cells result in the activation of the adaptive immune responses [90]. It is this ability of a cell death mode to activate danger signaling pathways that culminate to the release of DAMPs with proinflammatory or immunomodulatory potential that distinguishes between ICD and tolerogenic cell death [91]. Ferroptosis, necroptosis and pyroptosis are examples of ICD mechanisms that can be induced through cancer treatment strategies [92]. On the other hand, apoptosis is regarded as non-ICD. Cells undergoing apoptosis preserve the cell membrane. Therefore, release of potentially immunogenic DAMPs does not occur. Also, cells undergoing apoptotic cell death express 'find me' signals such as phosphatidylserine and release immunosuppressive cytokines such as interleukin (IL)-10 and transforming growth factor-beta (TGF-β) [61]. The phagocytic cells respond to apoptosis by identifying the 'find me' phagocytosis signals and eliminate the dead cells without stimulation of inflammatory responses [93]. In this context, apoptosis is relevant to physiology in the removal of unwanted cells as ICD would create pathological conditions and harm homeostasis.

Compelling evidence has been found which supports that the propensity to undergo ICD is a prognostic factor associated with longer survival in cancer patients generally, GBM patients included [94]. Furthermore, it has been observed that the higher the ICD propensity, the stronger the anti-tumor immune response. A strong tumor response in turn is more effective in the combating and slowing down of tumor growth [95]. This scenario would be expected in highly heterogenous pictures such as the one in GBM. However, how GBM exhibits heterogeneity and still exhibits a cold tumor microenvironment that blunts responses to potentiate ICD-inducing cell death mechanisms is still not fully understood.

Depending on cell types, glioma cells undergo various mechanisms of cell death following TK/GCV suicide gene therapy. In several previously conducted studies, apoptosis has been reported to be the cell death mechanism occurring in glioma cell lines such as LN-18, LN-229, U87, 9L and T98G [50, 96]. In another study conducted using Chinese hamster ovary (CHO) cell line, more than one mechanism of cell death was seen to be activated (apoptosis and necrosis (<10%)) following TK/GCV suicide gene therapy [97]. Notably, no published data has been reported for cell death mechanism undertaken by GL261 and CT2A following TK/GCV suicide gene therapy and how they respond to TK/GCV upon interruption of the apoptotic pathway.

Chapter 2

2 Study aims

The unique and challenging characteristics of GBM have been reviewed and discussed in Chapter 1. However, little is known about the different types of cell death GBM cells can undergo which is also very important in the context of treatment. Following cancer therapy, cancer cells can be eliminated through apoptosis or other possible cellular responses which include caspase independent apoptosis or ICD modes of cell death [98]. In this project, HSV-TK/GCV treatment will be used as a model treatment to induce apoptosis. The overall aim of the thesis is to better understand how and if GBM cells die when apoptosis is blocked. An in depth understanding of the diverse modes of cell death has a huge potential to open new perspectives for the treatment of cancers by providing a molecular basis for novel strategies targeting cell death pathways in resistant cancers. Therefore, the objectives of this thesis work are:

- to investigate the apoptotic pathway in GBM following HSV-TK/GCV suicide gene therapy.
- to block the apoptotic pathway and study potential escape death pathways following HSV-TK/GCV SGT.

Chapter 3

3 Materials and Methods

3.1 Clustered Regularly Interspaced Short Palindromic Repeats (CRISPR) and CRISPR-associated protein 9 (CRISPR-Cas9) Lentiviral vector designing

The lentiviral CRISPR plasmids targeting the gene x and gene y genome locus (due to potential IP conflicts, official gene names cannot be mentioned) were designed according to the Genome-scale CRISPR Knock-out(KO) (GeCKO) protocol by the Zhang lab [99, 100]. The lentiCRISPRv2 plasmid (one vector system) containing both humanized *S.pyogenes* gene X (hSpgene X) and chimeric guide RNA was used in designing the transfer vector. This is as illustrated in Figure 3.1.

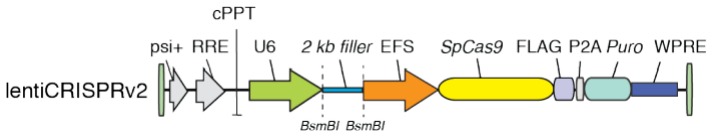

(**a**)

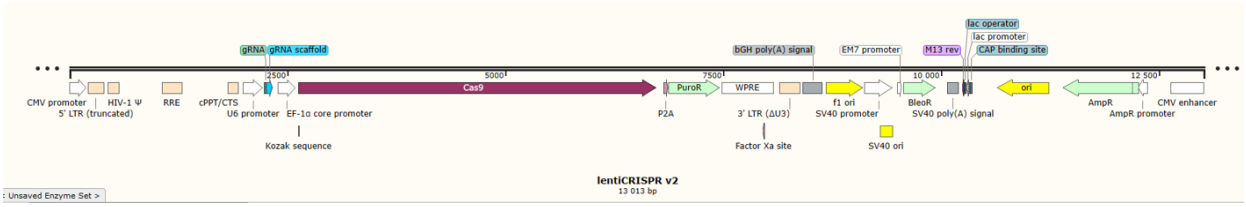

(**b**)

Figure 3.1: LentiCRISPRv2 plasmid map (**a**) shows the site at which annealed oligos ligate to the lentiCRISPRv2 following its digestion with *BsmBI*, (b) shows the guide RNA, the puromycin and ampicillin resistant genes that were utilized in the selection of transformed bacteria and transduced cells respectively. Fig (**a**) derived from [99, 100] and (**b**) Addgene plasmid #52961, Feng Zhang [99]

5 µg of lentiviral CRISPR plasmid (Addgene) were dephosphorylated using Fast alkaline phosphatase (FastAP) (Fermentas, USA) and digested with FastDigest *BsmBI* restriction enzyme (Fermentas, USA) for 30 minutes at 37°C to create the ligation sites. 100Mm Dithiothreitol (DTT) was added as a reducing agent and 10X FastDigest Buffer (Fermentas, USA), was added to provide

a conducive environment for digestion to take place. The digested plasmid was gel purified using the QIAquick Gel Extraction Kit (QIAGEN, Germany) while following manufacturer's protocol, eluted in elution buffer and its concentration measurement done using a nanodrop spectrophotometer (ND-1000, Nanodrop Technologies, USA).

Following that, 100 µM of each oligo was prepared in a PCR reaction tube. Thereafter, the respective forward and reverse oligos shown in Table 3.1 (i.e., for instance mGene x KO1 Fx and mGene x KO1 Rx) were matched, phosphorylated with T4 Polynucleotide kinase (PNK) (New England Biolabs (NEB) Ipswich, USA) in the presence of T4 PNK buffer (NEB, USA) supplemented with 1mM ATP. The gRNA sequences were derived from bioinfo analysis using an online platform from Broad institute found here:

https://portals.broadinstitute.org/gppx/crispick/public

Table 3.1: Gene x and Gene y gene primers/oligos

Primer/oligo	Sequence (5' to 3')	Catalogue #	Supplier
mGene x KO1.Fx	CAC CGC TTC ACG CGC GAC ATG ATC G	10336-022	Invitrogen, Thermo Fisher Scientific, USA
mGene x KO1.Rx	AAA CCG ATC ATG TCG CGC GTG AAG C		
mGene x KO2.Fy	CAC CGC TGG CTT CAC TCT TGC AAA G		
mGene x KO2.Ry	AAA CCT TTG CAA GAG TGA AGC CAG C		
mGene y KO1.Fx	CAC CGT ACA ACG CTC TGC TAC ACG A		
mGene y KO1.Rx	AAA CTC GTG TAG CAG AGC GTT GTA C		
mGene y KO2.Fy	CAC CGC CAA TTA AAG ACA CTA CAA G		
mGene y KO1.Ry	AAA CCT TGT AGT GTC TTT AAT TGG C		

The oligo pairs were then annealed in the EN 61326, Class A, Group 1 SimpliAmp Thermal Cycler (Life Sciences Technologies, Singapore). The annealing reaction was conducted as follows: firstly at 37°C for 30 minutes, then at 95°C for 5 minutes and finally ramped down to 25°C at a temperature drop rate of 5°C/min.

Resulting annealed oligos were then diluted with a dilution factor of 200 using nuclease free water prior to the ligation step. The ligation reaction was set up and left to incubate at room temperature for 10 minutes. The setup was as follows; 1µl of the diluted oligo duplexes was ligated to 50 ng *BsmBI* digested lentiCRISPRv2 plasmid using Quick ligase enzyme (NEB) in the presence of 2X Quick ligase buffer (NEB). The ligation product was used to transform bacteria and make plasmid

preparation. For quality control purposes, a negative control ligation was set up by substituting oligos with water in a separate PCR reaction tube.

3.2 Bacterial transformation

One Shot Stbl3 *E.coli* strain (Invitrogen, Thermo Fisher Scientific) was used according to manufacturer's protocol. One Shot Stbl3 chemically competent *E.coli* vials kept at -80°C were thawed on ice for 10 minutes and S.O.C medium (supplied with the kit) was warmed to room temperature. Thereafter, 1-5 µl of each of the recombinant Lentiviral transfer plasmids (10 pg to 100 ng) was added into separate 50 µl vials of One Shot chemically competent Stbl3 *E.coli,* gently mixed by swirling and incubated on ice for 30 minutes. The cells were then heat shocked at 42°C on a heat block without shaking, immediately transferred back on ice for 2 minutes followed by addition of 250 µl S.O.C medium (prewarmed to room temperature) to each vial. The vials were then shaken horizontally in a shaking incubator (4430, New Brunnswick Innova, Belgium) at 37°C for 1 hour at 225 rpm. Following that, 20 µl and 150 µl of each transformation solution was spread onto 2 separate Lennox Luria Broth (LB) (Invitrogen, USA) agar plates (pre-warmed to 37°C for 30 minutes in an incubator) and incubated overnight at 37°C in an inverted position. Lennox LB agar was prepared by adding 32 grams of Lennox LB agar powder (Sigma, USA) per litre of distilled water and autoclaved at 121°C for 15 mins. Agar was left to cool down to 60°C, supplemented with 100 µg/ml of ampicillin (Sigma Aldrich, USA), poured in sterile culture plates, left to solidify at room temperature and kept at 4°C.

Following overnight incubation, single colonies were randomly picked from all the plates using sterile inoculation loops and each colony was sub-cultured in a 15 ml falcon tube containing 6 ml of Muller's LB (Invitrogen, USA). Miller's LB preparation was done by adding 25 grams of Muller's LB Broth base per litre of distilled water followed by 15 minutes of autoclaving at 121°C. Thereafter, broth was cooled down at room temperature and kept at 4°C. Prior to use the broth was supplemented with 100 µg/ml ampicillin. The whole bacterial culture procedure was performed under a sterile environment induced using a bunsen burner. A single falcon tube containing ampicillin deficient LB medium only, was included as a negative control. Falcon tube lids were loosely capped and incubated while shaking horizontally at 37°C overnight at 225rpm in a shaking incubator. Thereafter, bacteria storage vials were prepared by adding 300 µl of 50% glycerol and

700 ul of LB bacterial culture in a cryopreservation tube and kept at -80°C. The falcon tubes were then centrifuged at 10°C for 10 minutes at 4000 rpm in a benchtop centrifuge. The supernatant was discarded, and plasmid DNA isolated from the bacterial pellets using the HQ Mini Plasmid Purification Kit (Invitrogen, Thermo Fisher Scientific, USA) according to the manufacturer's provided protocol. To determine the plasmid DNA concentration in each colony, the nanodrop spectrophotometer (ND-1000, Nanodrop Technologies, USA) was used. To confirm if the cloning was successful, 5 µg of each knock-out DNA construct sample was sent as dried spots on filter paper to Synbio Technologies, USA for Sanger DNA sequencing.

3.3 Cell culture

During cell culture work, asceptic techniques were practiced and all work was conducted inside a laminar airflow hood (Class II S2010 1.2 EN, Heto-Holten, Denmark and ninoSAFE Class II 1200, Nino Labinterior, Sweden) to achieve a sterile environment. The laminar flow hood was disinfected with 70% ethanol before and after conducting experiments. All work surfaces, equipment and instruments were disinfected with 70% ethanol prior to use. Throughout the work, all 37°C cell incubations were done in a 5% CO_2 humidified cell culture incubator (Thermo Scientific Forma 3111, USA and Thermo Forma 371, USA) set at 37°C. Following every old media removal step, cells were washed with sterile Dulbecco's phosphate buffered saline (DPBS) prepared by a 1:10 dilution of stock DPBS (Sigma Aldrich, USA) with sterile milli-Q water (referred throughout to as 1XPBS). Cell growth was monitored using the Olympus CK-X31SF light microscope (Olympus Optical, Japan) and Eclipse TS100-F Trinocular Inverted fluorescence microscope (Nikon).
Experimental analyses were carried out in vitro using the following cell lines obtained from the Miletic lab:

(i) **U87:** a human derived cell line from a female patient who was suffering from pleomorphic GBM that is commonly used as an experimental model of GBM [101].

(ii) **CT2A:** a mouse glioma cell line derived from a sub-cutaneous and non-metastatic astrocytoma. CT2A cells are useful in therapeutic research on brain malignancies [102].

(iii) **Mouse glioma 261 (GL261):** murine glioma cells derived from syngeneic mouse.

(iv) **Human embryonic kidney 293 (HEK 293):** HEK293 is a human derived cell line that is extensively used in research for viral vector production due to its high transfection efficiency [103].

3.3.1 Media preparation

Unless otherwise stated, all cell lines were cultured in Dulbecco's Modified Eagle's Medium (DMEM) (Sigma Aldrich, USA) cell culture medium which was supplemented with 10% heat-inactivated FBS (Gibco, Life Technologies Limited, Brazil), Penicillin-Streptomycin 2% (v/v) (Lonza, BioWhittaker, Belgium), 2% (v/v) L-glutamine (BioWhittaker, Belgium), 3.2% non-essential amino acids (NEAA) (Lonza, USA), and 0.02% Plasmocin (Invitrogen, France). This culture media is referred to throughout the thesis as complete DMEM. Cryopreservation media was prepared by supplementing the complete DMEM with 10% (v/v) fetal bovine serum (FBS) (Gibco, Life Technologies, Brazil) and 10% (v/v) dimethyl sulfoxide (DMSO) (Sigma Aldrich, USA) and kept on ice. Fresh cryopreservation medium was prepared all the time prior to use. All tissue culture flasks, cell culture plates, cryogenic vials and cell strainers were purchased from Thermo Fisher Scientific, USA.

3.3.2 Preparation of drugs

Raptinal (a rapid-caspase activator) and Ganciclovir (GCV) were used to induce cell death whilst puromycin was utilized in cell selection. Preparation of the drugs was as follows:

Raptinal: Stock concentrations of 25 mM were prepared by dissolving raptinal (Sigma Aldrich, USA) in DMSO and kept at 4°C. Experiments were conducted using 10 µM raptinal prepared by further dilution of the 25 mM stock vials with complete DMEM.

Puromycin: Stock concentrations of 10 mg/ml were made by dissolving puromycin (Sigma Aldrich, USA) in complete DMEM and kept at -20°C. For the experiments, working concentrations of 0.5 µg/ml, 1.0 µg/ml and 1.5 µg/ml were prepared by further dilution of the stock vials with complete DMEM.

Ganciclovir (GCV): Stock concentrations of 3 mM were prepared by dissolving GCV (Sigma Aldrich, USA) in complete DMEM and kept at -20°C. Experiments were conducted using 20 µM concentration prepared by further stock dilution with complete DMEM.

3.3.3 Cryopreservation and thawing of cells

Cells were frozen down upon reaching ~ 80% confluency in a cell culture flask. Firstly, the old media was aspirated and discarded, followed by a cell wash step using 1XPBS prepared as described in section **3.3**. The 1XPBS was removed and cells were trypsinized by adding 1-2 ml of trypsin-ethylenediamine tetraacetic acid (EDTA) (EuroClone, Italy) prewarmed at room temperature and culture flask was incubated at 37°C. Following that, trypsin activity was stopped by resuspending the cells in complete DMEM (at least 3 times the volume of trypsin-EDTA used for trypsinization). The cell suspension was transferred into a falcon tube for centrifugation at 900 rpm for 5 minutes. The supernatant was discarded, and cell pellets were re-suspended in cold cryopreservation media prepared as described in section **3.3.1**. The cell suspension was aliquoted in 1ml cryopreservation tubes, and the tubes were immediately transferred into the Mr Frosty ™ Freezing container (Sigma Aldrich, Germany) and kept at -80°C overnight. After that, the cryopreservation tubes were taken out of the Mr Frosty ™ and further kept at -80°C until later use. For long term storage cells were kept in a nitrogen tank.

During cell thawing, the cryovials with frozen cells were transported on ice from -80°C storage freezer and warmed for 2-5 minutes at 37°C in a water bath. Thereafter, cells were washed by re-suspending them in 5-7 ml of pre-warmed complete DMEM in a 15 ml falcon tube and then centrifuging the falcon tube at 900 rpm for 5 minutes. After centrifugation, the supernatant was discarded, cell pellets were re-suspended in 4 ml or 12 ml of DMEM complete and then transferred into a cell T25 or T75 culture flask, respectively. The cell culture flask was then incubated at 37°C and cell growth constantly monitored using a light microscope until cells reached ~80% confluency.

3.3.4 Cell splitting

Upon reaching ~ 80% cell confluency, old media was discarded, and cells were washed and trypsinized as described in **3.3.3**. The cells were gently resuspended in 5 ml prewarmed complete DMEM. The desired volume of cell suspension was retained into the flask and the total media volume was topped up to 4 ml and 12 ml in a T25, and T75 cell culture flask, respectively. The flasks were then incubated at 37°C. Alternatively, when a specific number of cells was to be re-cultured, a viable cell count was done to determine the cell suspension volume to be retained in the flask.

3.3.5 Cell counting

Cells were manually counted using the Neubauer cell counting chamber (Thermo Fisher Scientific, USA). Trypan blue (Sigma Aldrich, USA), a viability stain was used to differentiate between live and dead cells. An equal volume of cell suspension and trypan blue was gently and thoroughly homogenized by up and down pipetting in an eppendorf tube. To determine the number of cells in 1 ml cell suspension, 10 µl of the cell suspension and trypan blue mixture was transferred onto the hemocytometer using a pipette. Viable cell count was immediately done using a light microscope. The cells in the large corner squares of the Neubauer cell counting chamber were countered and within each square, only the cells lying on the top and right edges of the square were counted, whilst the cells lying on the left and bottom edge of the square were excluded from the count. The total cell count in 1 ml of cell suspension was calculated using the formula:

$$Number\ of\ cells\ in\ 1\ ml\ cell\ suspension = \frac{total\ number\ of\ cells\ counted}{number\ of\ large\ corner\ squares\ counted} * 10^4 * dilution\ factor$$

3.4 Viral production and viral transduction

The Lentiviral particles were produced, collected and concentrated according to the protocol published previously [104]. Plasmids shown in Table 3.2 were added into 1 ml prewarmed Optimem 1 (Invitrogen Life sciences, USA).

Table 3.2: Plasmids used for lentiviral particles' production

Plasmid	Plasmid amount (µg)
pGene X KO or pGene Y KO	5.6
pMDLgpRRE	4.8
pRSV-Rev	2.4
phCMV-VSV-G	1.2

X-treme GENE 9 DNA transfection reagent (Roche Diagnostics, Germany) was used to efficiently transfect HEK 293 T cells with the Lentiviral particles. The L-70 ultracentrifuge (Beckman Coulter, USA) was used for ultracentrifugation during the lentiviral particles' concentration procedure.

Following concentrated lentiviral particles' production, U87, CT2A and GL261 cell lines were seeded at a density of 5×10^4 cells in 500 µl DMEM media (in duplicates) in separate wells of a 24-well plate and incubated overnight at 37°C. The following day, one well of each cell type was transduced with 10 µl of thawed concentrated lentiviral particles. U87 cells were included as a positive control as U87 cells are known to be efficiently transduced with lentivirus [105]. Thereafter, the 12-well plate was wrapped around with paraffin film and centrifuged at 31°C, for 1.5 hours at 2250 rpm to facilitate spinoculation. The plate was placed inside an incubator at 37°C, and cell growth monitored until the cells reached approximately 80% confluency. Thereafter, the cells were expanded and spilt into three different T25 cell culture flasks.

To select transduced cells, the puromycin gene encoded by the lentiviral particles was utilized. The cells in the three T25 cell culture flasks were treated with 0.5 µg/ml, 1.0 µg/ml, and 1.5 µg/ml puromycin concentrations. For each cell line, wild type cells were included as control and treated the same way. The cells were subjected to puromycin for 7 days with regular media changes. Puromycin concentration of 1.0 µg/ml was selected as the optimum concentration. Thereafter, the viable puromycin resistant cells were expanded. To verify and confirm successful gene x KO of CT2A and GL261 cells, the western immunoblotting technique was utilized whilst blotting against gene x antibodies. Further screening of cells was done to isolate single cell clones with total gene knockdown using the limiting dilution cloning method. Here, 0.5 cells per well were sub-cultured in 96-well plates in 200 µl DMEM media. Upon reaching ~80% cell confluency, random clones

were selected, expanded, and analyzed through western blotting to confirm knocking out of the gene of interest (gene x).

After that, a single gene x knocked out clone from both CT2A and GL261 cells was selected and transduced with 2 µl of lentiviral particles encoding TK.007-GFP (provided by Dr. Hossain, University of Bergen). Virus addition was followed by spinoculation as already described above. To isolate TK.007-GFP lentivirus transduced cells, cell sorting was performed using the SH 800 cell sorter (Sony Biotechnology, USA). Cell preparation for cell sorting was done by trypsinizing cells, suspending them in 10 ml DMEM and transferring them into a falcon tube while straining them with a 70 µl sterile cell strainer to get singe cells. The falcon tube was spun at 900 rpm for 5 minutes and supernatant was discarded. Cell pellets were resuspended in 1.5 ml DMEM media and kept on ice until they were processed in the cell sorter. Thereafter, the TK.007-GFP lentivirus positive cells were washed three times by centrifugating the cells and re-suspending them in fresh DMEM media. Following the final wash, the cells were seeded in a T25 cell culture flask and expanded.

3.5 Determination of cell death time points following Raptinal and GCV drug treatments

To determine the time points at which cells were non-viable following 10 µM raptinal and 20 µM GCV treatments, the Incucyte® live cell imaging system (S3 Sartorius, Germany) and WST assay technique were utilized. A cell density of $50x10^3$ cells in 500 µl complete DMEM were seeded in a 24-well cell culture plate and incubated overnight. The following day, old media was discarded and replaced with complete DMEM supplemented with either 10 µM raptinal or 20 µM GCV and immediately incubated in the Incucyte® S3 system live cell imaging analyzer for the required period. Thereafter, images acquired at 20× objective were analyzed using the Incucyte® S3 software.

A cell density of $15x10^3$ cells in 100 µl complete DMEM was seeded in each well of a 96-well cell culture plate and incubated overnight. Following that, cells were treated with either (20 µM GCV or 10 µM raptinal) for the required period. After that, 10 µl cell proliferation reagent WST-1 (Roche, Germany) was added into each well and microplate incubated at 37°C for 1-2 hours. The

absorbance was then measured at 450 nm using the Multiskan FC 357 microplate photometer (Thermo Fisher Scientific, China).

3.6 SDS-PAGE and Western immunoblotting

3.6.1 Preparation of cells

The cells were detached from the cell culture flask surface using sterile cell scrapers and transferred into 15 ml falcon tubes for 5 minutes centrifugation at 4°C and 3000 rpm. The cells were kept on ice throughout all the following procedures. The supernatant was discarded, and cell pellets were re-suspended in 1 ml 1XPBS and centrifuged for 5 minutes at 4°C and 3000 rpm. The supernatant was then discarded, followed by resuspension of cell pellets in 50-75 µl ice cold mammalian protein extraction reagent (Thermo Scientific, USA) supplemented with 10% (v/v) protease inhibitor (Roche Diagnostics, Germany) and 10% (v/v) phosphatase inhibitor (Roche Diagnostics, Germany). The cell pellet suspension was transferred into an eppendorf tube and left on ice for 30 minutes with light spins after every 10 minutes. Thereafter, the cell lysate was centrifuged at 4°C for 10 minutes at 14 000 rpm. The supernatant was collected into a fresh eppendorf tube, and protein concentration determination was done using the Pierce bicinchoninic acid (BCA) Protein Assay kit (Roche Diagnostics, Germany) whilst following the manufacturer's protocol. For storage, the supernatant was kept at -80°C. Bovine serum albumin (BSA) (Aldrich Sigma, USA) of concentrations; 10 mg/ml, 5 mg/ml, 2.5 mg/ml, 1.25 mg/ml, 0.625 mg/ml, and 0.3125 mg/ml together with milli-Q water (0 mg/ml) were used in plotting the linear standard graph against which the samples' protein concentrations were calculated. Protein photometric absorbance measurements were done using a Multiskan FC 357 microplate photometer (Thermo Fisher Scientific, China) at 560 nm.

For proteins to resolve according to their molecular weight during sodium dodecyl sulfate (SDS)-polyacrylamide gel electrophoresis (PAGE), sample denaturation and reduction is crucial. Protein lysate samples were reduced and denatured using Nupage sample reducing agent (10x) (Invitrogen, USA) and Nupage lithium dodecyl sulfate (LDS) sample buffer (4x) (Invitrogen, USA) respectively. Following addition of the reducing agent and denaturant to protein lysates in an

eppendorf tube, the eppendorf tube was shortly vortexed to mix the contents, heated at 70°C for 10 minutes to aid in the denaturation and immediately placed back on ice for ~ 10 minutes.

3.6.2 SDS-PAGE

Hand cast SDS-polyacrylamide gel of 1.5 mm thickness, consisting of 10% polyacrylamide resolving gel and 4% polyacrylamide stacking gel was prepared using the Mini-PROTEAN Tetra Hand-Cast System (Biorad, USA). The concentrations of 30% Acrylamide/Bis-acrylamide solution (Sigma Aldrich, USA), 1.5 M Tris-HCl (pH 8.8), 1.0 M Tris-HCl (p H 6.8), 10% Sodium dodecyl sulfate (SDS) (w/v), 10% ammonium persulfate (APS) (Sigma Aldrich, USA), and Tetramethylethylenediamine (TEMED) (Sigma Aldrich, USA) used in gel casting are summarized in Table 3.3.

Table 3.3: SDS-polyacrylamide gel preparation for protein electrophoresis

	Component concentration% (v/v)	
Solution component	**Resolving gel**	**Stacking gel**
30% Acrylamide/Bis-acrylamide solution	34	17
1.5 M Tris-HCl (pH 8.8)	26	-
1.0 M Tris-HCl (pH 6.8)	-	13
10% SDS	1	1
10% APS	1	1
TEMED	0.04	0.1

The cast SDS-polyacrylamide gel was placed inside the electrophoresis chamber before filling it up with electrophoresis buffer**.** Preparation of electrophoresis buffer was done by diluting 10x Tris/glycine (Biorad, USA) with deionized water using a dilution factor of 10. Thereafter, 20-30 µg of each sample and 10 µl SeeBlue Plus2 Pre-Stained Protein Standard (Invitrogen, Thermo Fisher Scientific, USA) was loaded into the wells of the SDS-polyacrylamide gel. SDS-PAGE was conducted using an electrophoresis power pack (Biorad, USA) at 70V until all samples had migrated to the bottom of the stacking gel (20-30 minutes). Further protein separation was done at 100V for 1 hour with the pre-stained molecular weight protein ladder serving as an indication of successful protein seperation.

3.6.3 Western immunoblotting analysis

Protein separation was followed by protein transfer onto a 0.2 µm nitrocellulose membrane (Cytiva, UK) using the *XCell SureLock* Mini-Cell (transfer chamber) (Invitrogen, USA) and *XCell II* Blot Module (transfer cassette) (Invitrogen, USA). Prior to protein transfer, the stacking gel was removed, and the resolving gel equilibrated in cold transfer buffer for ~ 2 minutes. Transfer buffer was prepared by adding Tris/glycine (Biorad, USA), methanol and deionized water at 1:2:7 volume ratio. The nitrocellulose membrane, Whatman filter paper (GE Healthcare, UK) and sponges used during assembly of the transfer stacks were soaked in cold transfer buffer for ~3 minutes before use, for them to equilibrate. A blotting roller was used to gently remove trapped air bubbles while assembling transfer stacks in wet tank transfer cassette. The transfer chamber was filled with cold transfer buffer and placed on ice. Following that the transfer cassette was placed inside the transfer chamber and protein transfer was run for 90 minutes at 30V supplied by the PS0301 PowerEase 300 W power supply (Life technologies, Carlbad, CA).

3.6.4 Protein detection

Protein transfer efficiency was assessed using Ponceau S solution (Sigma Aldrich, USA). The nitrocellulose membrane was washed with milli-Q water, incubated in Ponceau S for 5 minutes at room temperature, and protein bands were visually assessed before rinsing the nitrocellulose membrane twice with milli-Q and keeping it wet in 1X tris buffered saline (TBS) supplemented with 0.1% Tween 20 (Sigma Aldrich, USA) (TBST). The TBST was prepared by diluting TBS (10X) buffer with deionized water using a dilution factor of 10. Following that, nitrocellulose membrane was blocked with blocking buffer (5% (w/v) skim milk powder (Sigma Aldrich, USA) dissolved in TBST) for 1 hour on tilting, at room temperature. The nitrocellulose membrane was then incubated with diluted primary antibodies overnight at 4°C, on tilting. Following that, the membrane was washed with TBST 3 times for 5 minutes on tilting, before incubating the membrane with horseradish peroxidase (HRP) conjugated secondary antibodies at room temperature for 1 hour on tilting. The primary and secondary antibodies, together with the dilution buffer used are summarized in Table 3.4. The membrane was washed with TBST 3 times for 5 minutes on tilting and covered with Super signal chemiluminescent substrate (Thermo Scientific, USA) for 5 minutes before measuring the chemiluminescence signal. Measurement and imaging of the

chemiluminescent signals (blot images) was done using the LAS 3000 luminescent image analyzer (Fujifilm, Medical Systems, USA). The acquisition and further analysis of blot images was performed using Image Lab and ImageJ softwares [106].

Table 3.4 Antibodies used during western immunoblotting

Primary antibodies	**Molecular weight (MW) kDa**	**Host**	**Dilution**	**Catalogue number**	**Supplier**	**Dilution buffer**
Caspase-3	~ 19 ~ 17	Rabbit	1:1000	9664S	Cell Signalling, USA	5% BSA TBST
Caspase-9	~49/39/37	Mouse	1:1000	9508T	Cell Signalling, USA	5% skim milk TBST
PARP-1	~ 116 ~ 89	Rabbit	1:1000	9542S	Cell Signalling, USA	5% BSA TBST
Beta actin	~ 42	Mouse	1:2000	Ab8224	Abcam, UK	5% skim milk TBST
Caspase-7	~ 20	Rabbit	1:1000	9491S	Cell signalling, USA	5% skim milk TBST
Secondary antibodies		**Host**	**Dilution**	**Catalogue number**	**Supplier**	**Dilution buffer**
Goat anti-mouse IgG (H+L), HRP		Mouse	1:5000	31430	Invitrogen, USA	5% skim milk TBST
Goat anti-Rabbit IgG (H+L), HRP		Rabbit	1:10000	31462	Invitrogen, USA	5% skim milk TBST

3.7 Propidium Iodide (PI) Uptake Assay

PI is a red fluorescent dye that binds to DNA. PI uptake assay is used to differentiate between cells with impaired membrane integrity and cells with an intact membrane. PI can enter necrotic cells as they are characterized by a ruptured membrane whereas in apoptotic cells ,PI uptake is excluded as the cells have an intact membrane [107]. In this work ,PI uptake was used to investigate induction of lytic cell death following HSV-TK/GCV SGT.

A cell density of $35x10^3$ cells in 500 µl complete DMEM was seeded in each well of a 24-well cell culture plate and incubated overnight. Following that, complete DMEM was replaced with 500 µl complete DMEM supplemented with 2.5 µg/ml PI solution (Biolegend, USA). This served as the

untreated control. Treated samples where replaced with 500 µl complete DMEM supplemented with 2.5 µg/ml PI solution and 20 µM GCV. After that, the cell culture plate was immediately incubated in the Incucyte® S3 system live cell imaging analyzer for the required period. Thereafter, images acquired at 20× objective were analyzed using the Incucyte® S3 software to calculate the red image mean. Data acquired from the Incucyte® S3 software was used to plot graphs in GraphPad prism software.

3.8 Data analysis

Data was analyzed using Excel and Two-way ANOVA followed by Tukey's multiple comparisons test which was performed using GraphPad prism version 9.5.1 for windows, GraphPad Software, San Diego, California USA, www.graphpad.com. A p value > 0.05 was considered as insignificant whereas p value < 0.05 was considered significant. Asterisks were used to represent the P values as follows; * , $p < 0.05$; ** , $p < 0.01$; *** , $p < 0.001$ and ****, $p < 0.0001$. Results were expressed as mean ± standard error measurement (SEM).

Chapter 4

4 Results

4.1 Validation of CRISPR/Cas9-mediated KO of gene x

Previously it was observed that CT2A and GL261 cells undergo intrinsic apoptotic cell death through cytochrome c release/caspase-9 activation following HSV-TK/GCV SGT (unpublished observation) (Figure 4.1).

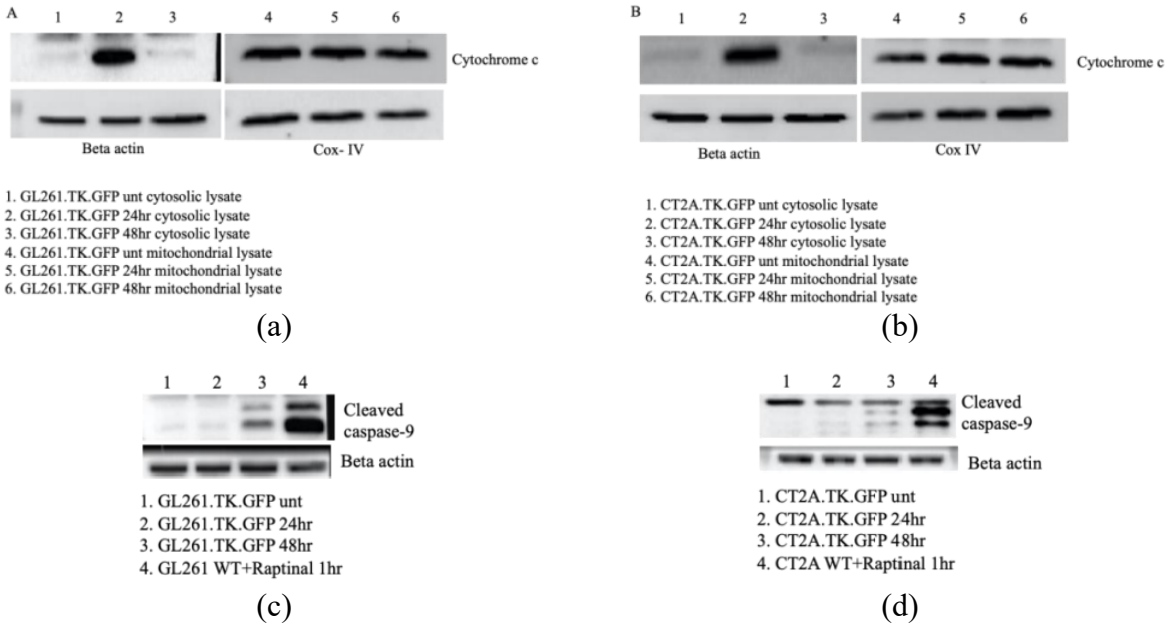

Figure 4.1: Caspase-9 activation in CT2A.TK GFP and GL261.TK GFP following HSV-TK/GCV SGT. GL261.TK.GFP (a, c) and CT2A.TK.GFP (b, d) were treated with 20 µM GCV up to 48 hours. Wild type (WT) CT2A and GL261 (CT2A.WT and GL261.WT, respectively) were treated with 10 µM raptinal for 1 hour (positive control). Untreated (unt) CT2A.WT and GL261.WT served as negative control. Cell lysates were prepared, and equal quantities of total protein were subjected to immunoblot analysis with antibodies to cytochrome c (a, b) and caspase-9 (c, d). Beta actin served as a loading control. Figure extracted from Shohana Afroz's Master thesis (2021), Department of Biomedicine, UIB.

In this work, we blocked the apoptotic pathway in CT2A and GL261 cells to examine potential activation of alternative death pathways following HSV-TK/GCV SGT. Blockage of the apoptotic pathway was performed through deletion of two important actors of the intrinsic apoptosis

pathway—hereafter referred to as gene x and gene y, to protect potential intellectual property rights. The deletion was achieved by using CRISPR/Cas9 technology. Due to time constraints, results in this thesis are focused on only one of the two genes, gene x. To confirm the successful deletion of gene x in CT2A and GL261, the bulk populations of these cells obtained after genome engineering were treated with 10 µM raptinal and immunoblotting was subsequently performed. Raptinal was used as it is known to be to be a rapid inducer of the caspase-dependent intrinsic apoptosis pathway [108].

Lack of detectable gene x cleavage (activation) products in the engineered CT2A and GL261 cells (referred to as CT2A gene x KO-bulk and GL261 gene x KO-bulk, respectively), indicated that the genome engineering was effective (Figure 4.2). However, faint bands (indicated in red rectangle) of a full-length gene x in both models were observed. This indicated the presence of cell populations with incomplete gene x KO. Therefore, we aimed to isolate single clones with complete deletion of gene x.

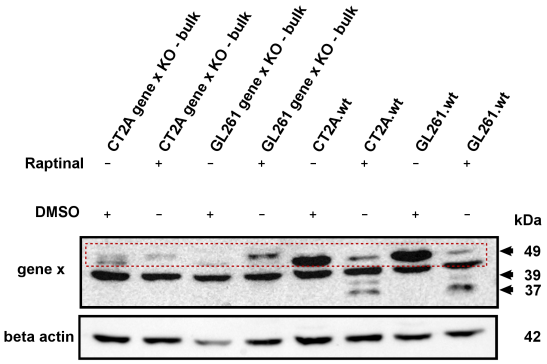

Figure 4.2: CRISPR/Cas9-mediated KO of gene x. CT2A and GL261 (wt and gene x KO-bulk) were treated with either 10 µM raptinal or DMSO (raptinal vehicle control) for 3 hours. Cell lysates were prepared, and equal quantities of total protein were subjected to immunoblot analysis with antibodies to gene x. The antibodies to gene x recognize both full length gene x and cleaved gene x products. The positions of the 49 kDa intact gene x (indicated in red rectangle) and the 39 kDa and 37 kDa cleavage product are indicated by arrows. Beta actin served as a loading control.

4.2 Generation of Single Cell–Derived Knockout Clones

To isolate clones with complete deletion of gene x from the bulk samples, limiting dilution method was performed. Eight clones from each cell line (i.e., CT2A gene x KO bulk and GL261 gene x KO bulk), were selected and subjected to immunoblot analysis with antibodies to gene x . In all

selected clones, gene x could not be detected (indicated in red rectangles) (Figure 4.3) which was indicative of successful isolation and expansion of gene x KO clones.

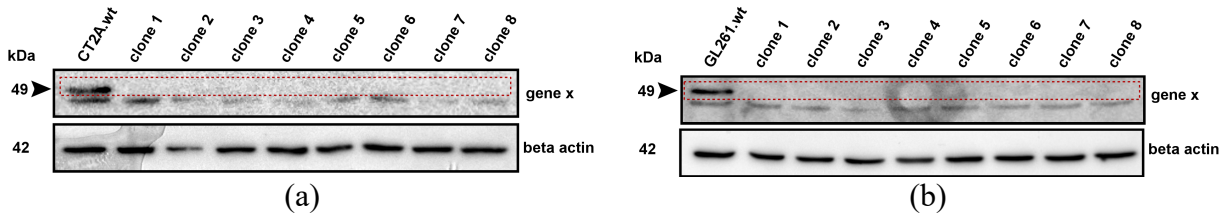

Figure 4.3: Generation of Single Cell–Derived gene x KO Clones. An equal number of CT2A.wt, CT2A gene x KO bulk-derived clones (a), GL261.wt and GL261 gene x KO bulk-derived clones (b) was seeded and incubated in DMEM overnight at 37°C. Thereafter, cell lysates were prepared, and equal quantities of total protein were subjected to immunoblot analysis with antibodies to gene x. The position of the 49 kDa intact gene x is indicated by arrows. CT2A.wt and GL261.wt served as positive controls whereas beta actin served as a loading control.

Three clones from CT2A (clone 1, 4 and 6) and GL261 (clone 2, 5 and 7) were randomly selected for the next analysis step to further isolate the clone showing the most efficient deletion of gene x. The CT2A clones (1, 4 and 6), GL261 clones (2, 5 and 7) , and their respective wt cells (CT2A.wt and GL261.wt, respectively) were treated with 10 µM raptinal and cell morphology was analyzed and compared at various time points using images obtained from the Incucyte® S3 system (Figure 4.4 and Figure 4.5).

While CT2A.wt and GL261.wt cells showed morphological changes suggestive of cell death as early as 3 hours following raptinal treatment, observation of similar changes was delayed in all the 3 selected clones for both CT2A and GL261. To select the most resistant clones to be used for all further experiments in both models, cellular morphology of the three clones was visually compared at 9 hours and 9.5 hours for the CT2A and GL261 model, respectively. The clone with cells that appeared morphologically viable at these time points was selected. Clone 1 (onwardly referred to as CT2A gene x KO) was elected amongst the CT2A clones and clone 2 (onwardly referred to as GL261 gene x KO) was selected amongst the GL261 clones.

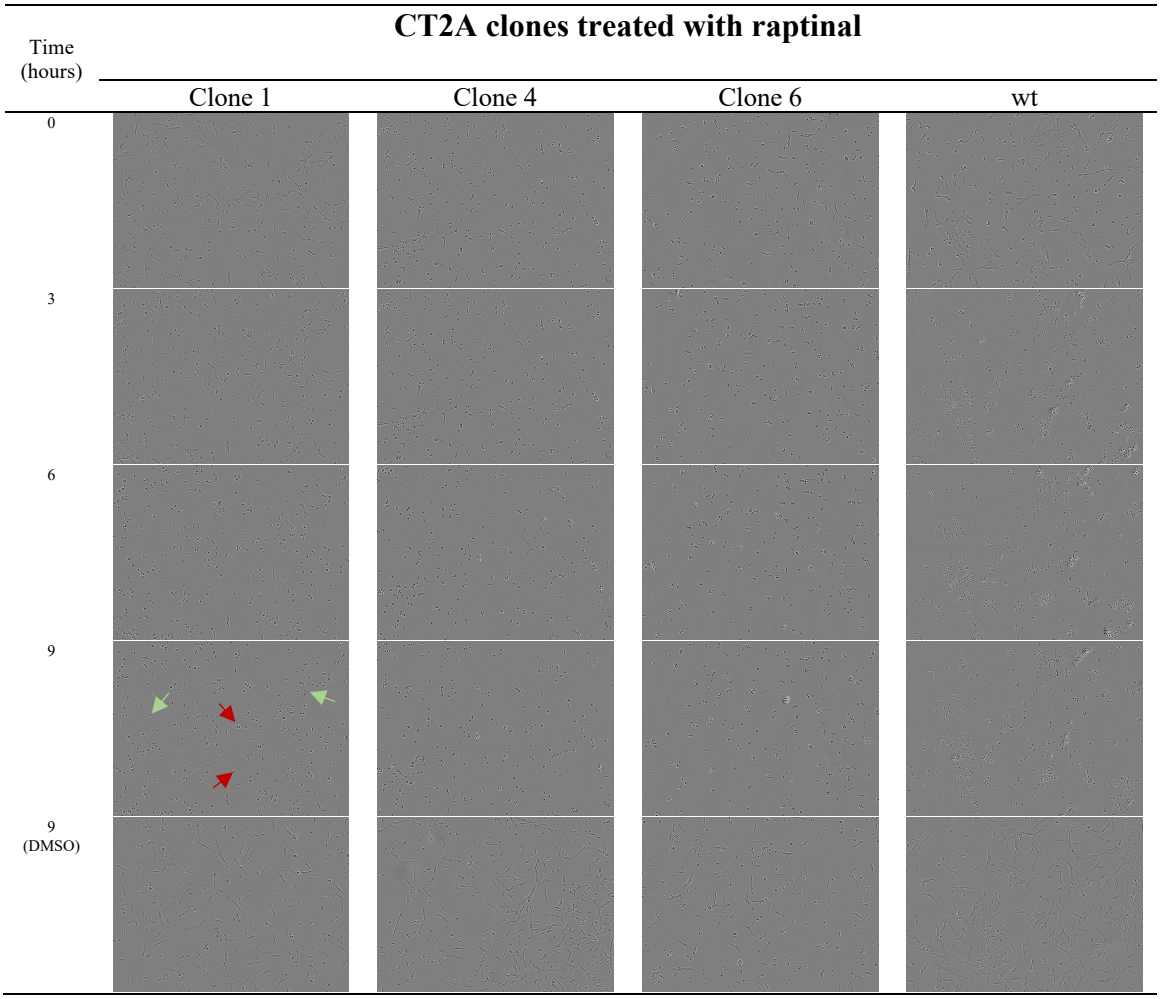

Figure 4.4: Raptinal cytotoxicity on CT2A gene x KO cells. CT2A.wt, and CT2A clones (1, 4 and 6) were treated with 10 µM raptinal for the indicated times. DMSO treated cells served as raptinal vehicle control. Morphologically viable and dead cells are indicated by green and red arrow, respectively). Real time cell morphological changes were captured using Incucyte ®S3 system at 10× objective. Better quality images can be accessed here: https://1drv.ms/f/s!Aj2lWAkKR6YU0RwGNSbjgqvQXrTS?e=jQckiL

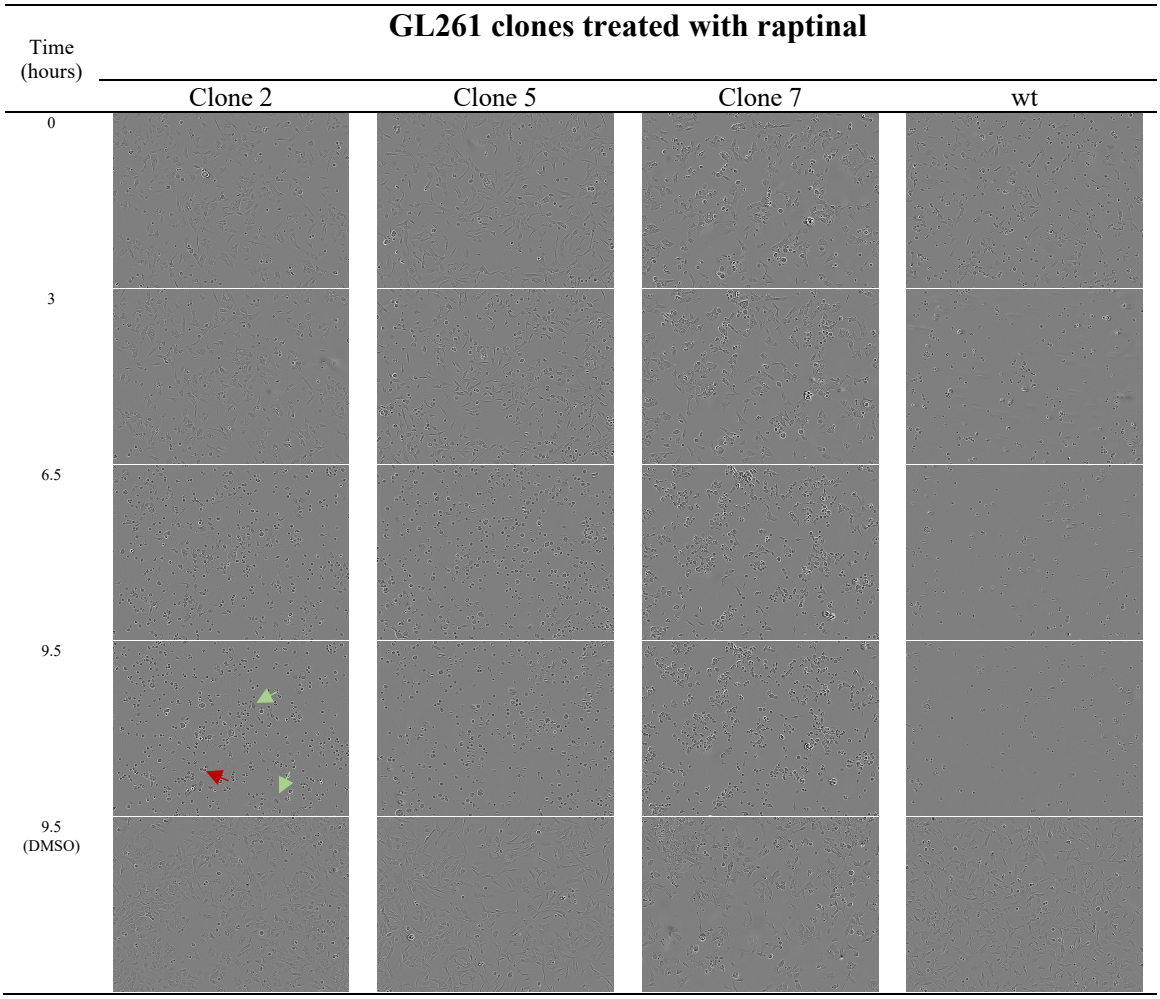

Figure 4.5: Raptinal cytotoxicity on GL261 gene x KO cells. GL261.wt, and GL261 clones (2, 5 and 7) were treated with 10 µM raptinal for the indicated periods of time. DMSO treated cells served as raptinal vehicle control. Morphologically viable and dead cells are indicated by green and red arrow, respectively. Real time cell morphological changes were captured using Incucyte® S3 system at 10× objective. Better quality images can be accessed here: https://1drv.ms/f/s!Aj2lWAkKR6YU0RwGNSbjgqvQXrTS?e=jQckiL

To further confirm the effect of knocking out gene x on cell death kinetics following raptinal treatment, WST cell viability assay was performed. Both CT2A gene x KO and GL261 gene x KO cells showed a significant delay in cell death, relative to CT2A.wt and GL261.wt, respectively (Figure 4.6). While treatment with raptinal for 3 hours reduced cell viability of CT2A.wt cells to~10% of control values, CT2A gene x KO cells showed resistance to raptinal-induced cell death and more than ~40% cells were found to be viable (Figure 4.6a). In GL261 gene x KO, ~80% of the control values were viable 3 hours down the raptinal treatment, in comparison to a reduced cell viability to ~40% of control values in GL261.wt (Figure 4.6b). These results, therefore, suggest that knocking out gene x interrupts the intrinsic apoptotic pathway in CT2A and GL261 following

raptinal treatment. They also suggest that CT2A cells are more sensitive to raptinal treatment than GL261 cells.

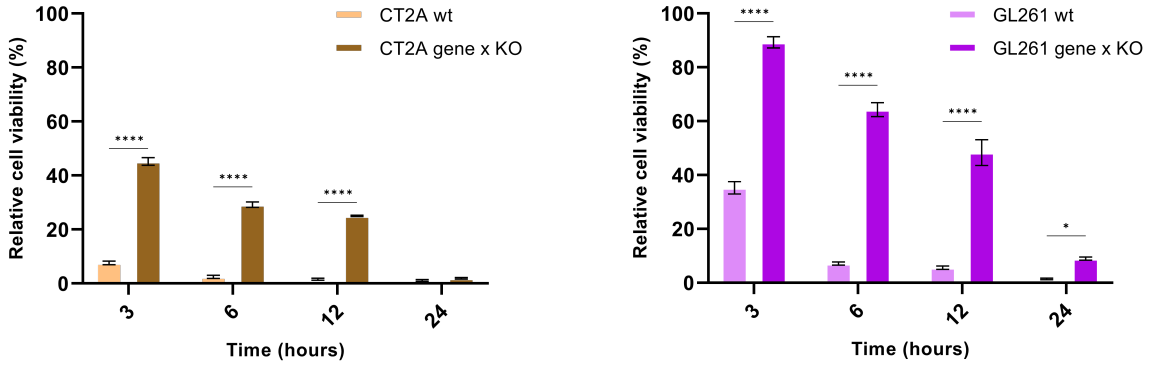

(a) **(b)**

Figure 4.6: Cell death kinetics in gene x KO cells following raptinal treatment. An equal number of CT2A.wt, CT2A gene x KO (selected clone 1), GL261.wt and GL261 gene x KO (selected clone 2) cells were treated with 10 µM raptinal for the indicated times. WST assay was used to determine the relative viable cells. At least 4 well replicates were included in each experimental condition. DMSO was used as a vehicle control (not shown). At every time point, each cell line was normalized to its DMSO vehicle control at the respective time point. The relative cell viability of CT2A gene x KO was compared to that of CT2A.wt **(a)** and GL261 gene x KO to that of GL261.wt cells **(b)**. Statistics were performed by Two-way ANOVA followed by Tukey's multiple comparisons test, * , $p < 0.05$ and ****, $p < 0.0001$. Non-significant comparisons not shown. The graphs and error bars were plotted with mean and SEM.

4.3 SGT-mediated cytotoxicity is reduced in gene x KO cells

To examine the effects of knocking out of gene x on cell death in CT2A and GL261 cells following HSV-TK/GCV SGT, CT2A.tk gene x KO, GL261.tk gene x KO, CT2A.tk and GL261.tk cells were generated by transducing CT2A gene x KO and GL261 gene x KO cells with lentiviral vectors encoding the HSV-TK gene [104]. After sorting the cells to ~98% purity and expansion, WST assay was conducted to quantify the number of viable cells at various time points following GCV treatment. Both CT2A.tk gene x KO and GL261.tk gene x KO showed a consistently higher viability at all time points than CT2A.tk and Gl261.tk, respectively (Figure 4.7). However, the difference is more pronounced in CT2A than GL261. A significant difference between CT2A.tk gene x KO and CT2A.tk was seen 48 hours post GCV treatment (Figure 4.7a). Similarly, between GL261.tk gene x KO and GL261.tk a significant difference was noted 48 hours post GCV treatment (Figure 4.7b). These results suggested that SGT-mediated cytotoxicity is obstructed by the deletion of gene x in CT2A and GL261 cells. They also suggested that CT2A cells are more sensitive to HSV-TK/GCV SGT than GL261 cells.

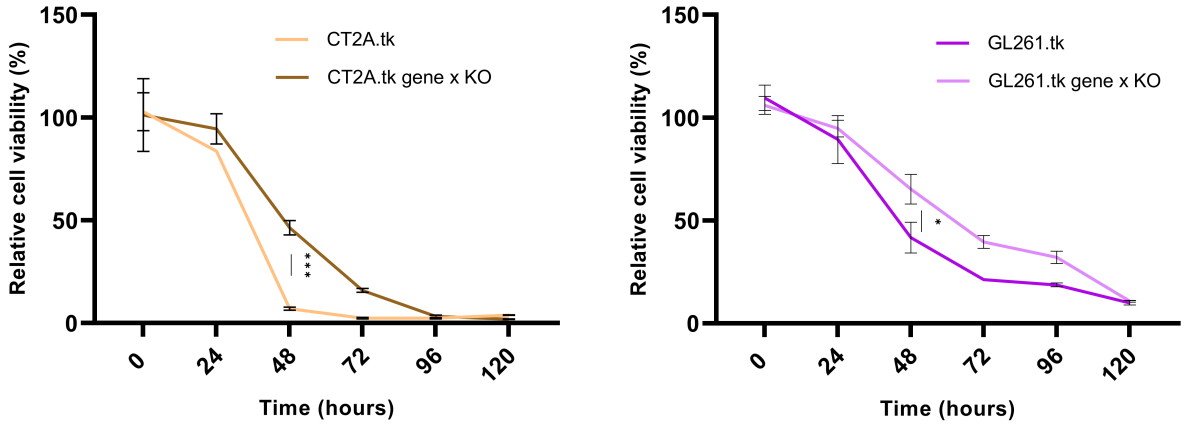

(a) (b)

Figure 4.7: Cell death kinetics in gene x KO cells following HSV-TK/GCV SGT. An equal number of CT2A.tk, CT2A.tk gene x KO, GL261.tk and GL261.tk gene x KO were treated with 20 µM GCV for the indicated periods of time. WST assay was used to determine the relative viability of cells. Four replicates were included in each experimental condition. DMEM was used as a vehicle control (not shown). At every time point, each cell line was normalized to its DMEM vehicle control at the respective time point. The relative cell viability of CT2A.tk gene x KO was compared to that of CT2A.tk **(a)** and GL261.tk gene x KO to that of GL261.tk cells **(b)**. Statistics were performed by Two-way ANOVA followed by Tukey's multiple comparisons test, * , $p < 0.05$, and ***, $p < 0.001$. Non-significant comparisons not shown. The graph and error bars were plotted with mean and SEM.

4.4 The Apoptotic pathway is interrupted following HSV-TK/GCV SGT in gene x KO cells

Following the observed changes in HSV-TK/GCV SGT cytotoxicity following gene x deletion, immunoblot analyses were performed to investigate induction of apoptosis in KO cells by HSV-TK/GCV SGT. First, activation of caspase-3 (an executioner caspase) in gene x KO cells was assessed at various time points following HSV/TK SGT. While cleavage of caspase-3 was clearly observed in wt cells, it was significantly reduced in gene x KO cells in both models (Figure 4.8a and Figure 4.8b).

To further confirm caspase-3 activation, cleavage of PARP-1 (an endogenous substrate of caspase-3) was assessed. The extent of cleavage of the full-length PARP-1 into cleaved fragments, increased with time from the start of GCV treatment, and it was clearly detected in CT2A.tk (Figure 4.8a). In a similar fashion, PARP-1 cleavage was also seen in GL26.tk, however, with a nearly constant cleavage through the entire period of GCV treatment (Figure 4.8b). At 96 hours, total PARP-1 cleavage was found in CT2A.tk as the full form PARP-1 could not be detected. These

results suggest that the intrinsic pathway of apoptosis is activated in CT2A.tk and GL261.tk following HSV/TK SGT, as already previously observed by our group (unpublished data). In CT2A.tk gene x KO, weak PARP-1 cleavage was detected with decreasing amounts of full-length PARP-1 as time elapsed post GCV treatment. Intriguingly, PARP-1 cleavage was not observed in GL261 gene x KO.tk cells at all time points. Thus, in Gl261, the inhibition of the apoptotic pathway seemed to be greater compared to CT2A due to the more pronounced inhibition of caspase-3 and PARP-1 cleavage.

To investigate whether the apoptotic pathway was induced through activation of caspase-7 (another executioner caspase), cleavage of caspase-7 was assessed. As shown in Figure 4.8, weak caspase-7 activation was seen in CT2A.tk and GL261.tk at 48 and 72 hours after GCV exposure whereas, in CT2A.tk gene x KO and GL261.tk gene x KO, cleaved caspase-7 could not be detected at all time points. Thus, collectively our data suggests that the apoptotic pathway is interrupted in gene x KO cells following HSV-TK/GCV SGT.

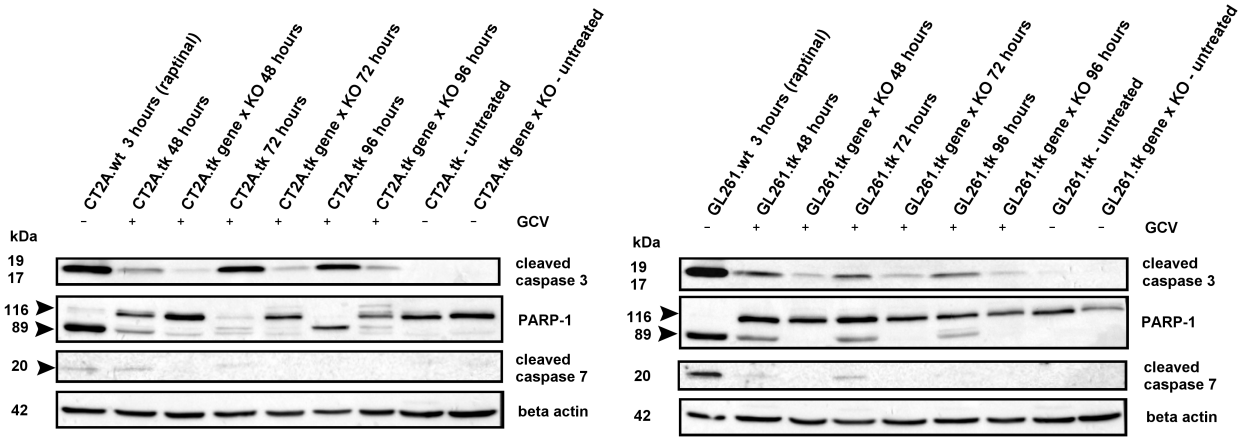

Figure 4.8: Investigation of apoptotic induction in gene x KO cells by HSV-TK/GCV SGT. CT2A (a) and GL261 (b) cells were incubated for indicated periods of time in raptinal (positive control), DMEM (negative control) or 20 μM GCV, after which cell lysates were prepared, and equal quantities of total protein were subjected to immunoblot analysis with indicated antibodies. The positions of respective antibodies blotted to are indicated by arrows. Beta actin served as a loading control.

4.5 Morphological characterization of cell death in the gene x KO cells

To investigate if there are morphological differences between CT2A.tk, GL261.tk, CT2A.tk gene x KO and GL261.tk gene x KO cells undergoing SGT induced cell death, real time cell morphological changes were visualized using Incucyte® S3 system derived images following GCV

treatment. Bubble-like protrusions are known to appear on the surface of dying cells that undergo cell death by membrane-rupture [109]. This morphological feature, that is suggestive of lytic cell death was seen in all cell types (i.e., CT2A.tk, GL261.tk, CT2A.tk gene x KO and GL261.tk gene x KO) (Figure 4.9).

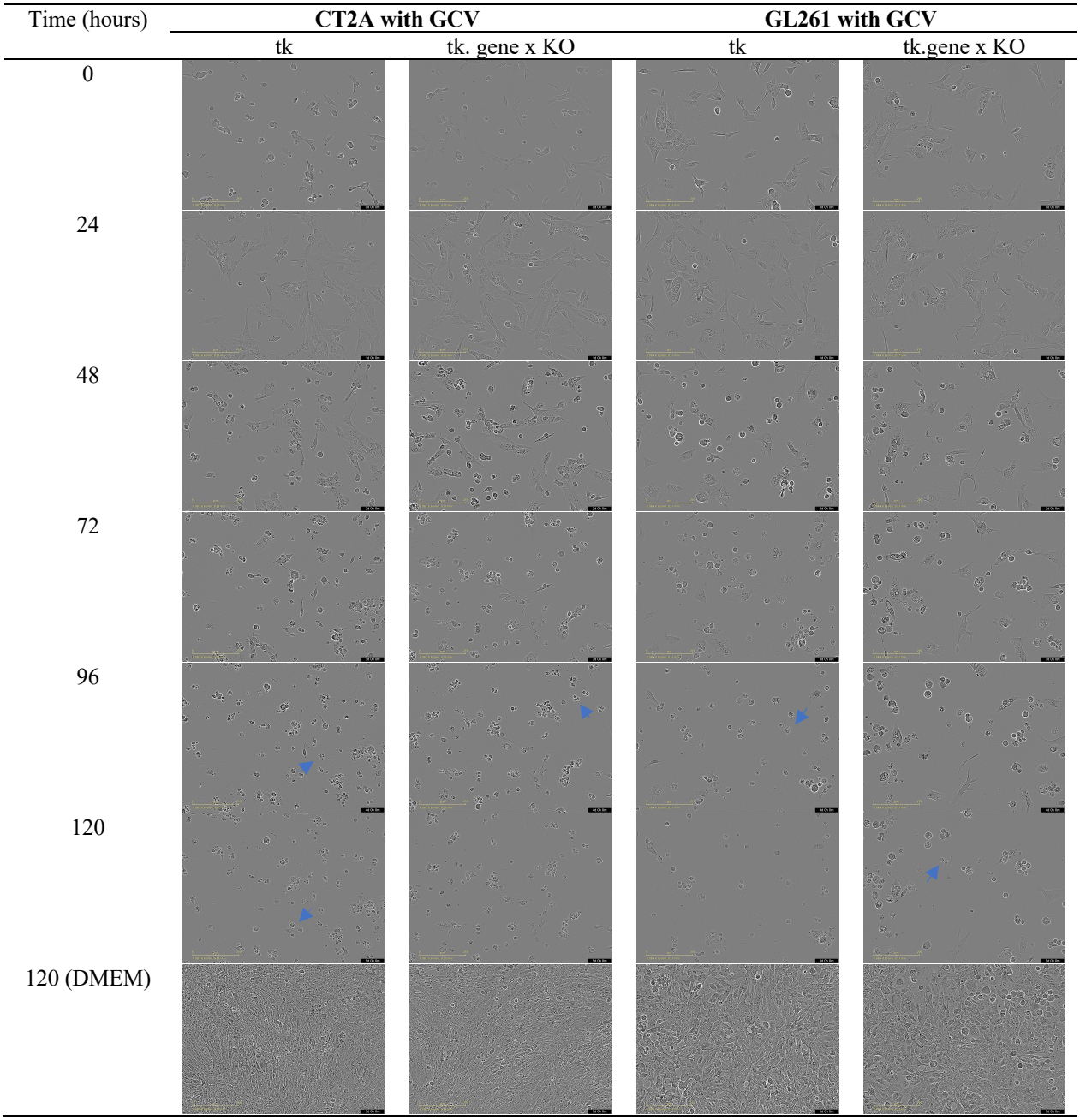

Figure 4.9: Morphological changes following HSV-TK/GCV SGT. An equal number of CT2A.tk, CT2A.tk gene x KO, GL261.tk and GL261.tk gene x KO were treated with 20 µM GCV for the indicated periods of time. DMEM treated cells served as GCV vehicle control. Bubble-like protrusions appearing on the cellular membrane surface of dying cells (lytic cell morphological feature) were seen (indicated by blue

arrows) and manually counted. The images shown are representative of three separate images, for each cell line used that were used for manual lytic cell quantification at each time point. Real time cell morphological changes were captured using Incucyte® S3 system at 20× objective. Scale bar: 200 µm. Better quality images can be accessed here: https://1drv.ms/f/s!Aj2lWAkKR6YU0RwGNSbjgqvQXrTS?e=jQckiL

To further assess the morphological changes continuously, videos were assembled using Incucyte® S3 software and visually assessed (Table 4.1).

Table 4.1: Videos illustrating cell morphological changes

Cell line	Link to video
CT2A.tk	https://1drv.ms/f/s!Aj2lWAkKR6YU0RwGNSbjgqvQXrTS?e=jQckiL
CT2A.tk gene x KO	https://1drv.ms/f/s!Aj2lWAkKR6YU0RwGNSbjgqvQXrTS?e=jQckiL
GL261.tk	https://1drv.ms/f/s!Aj2lWAkKR6YU0RwGNSbjgqvQXrTS?e=jQckiL
GL261.tk gene x KO	https://1drv.ms/f/s!Aj2lWAkKR6YU0RwGNSbjgqvQXrTS?e=jQckiL

The videos demonstrate morphological changes taking place at 30 minutes time intervals between 24 and 96 hours following GCV addition. A representative image for each cell line captured at 3 days 18 hours following GCV treatment was extracted to demonstrate the morphological differences observed in the videos (Figure 4.10). CT2A.tk and CT2A.tk gene x KO exhibited a similar heterogenous morphological picture in which typical apoptotic morphological features were seen (blue arrows). This included shrunken cells with rough edges suggestive of cell shrinkage and cellular blebbing. Additionally, lytic cell death was seen in both CT2A.tk and CT2A.tk gene x KO (red arrows). On the contrary, a major difference was observed between GL261.tk and GL261.tk gene x KO. In GL261.tk cells, only a few cells possess lytic cell morphology whereas most of the cells display apoptotic morphology at this time point. On the contrary, in GL261.tk gene x KO cells, seemingly swollen, round cells with smooth edges were seen (black arrows) in addition to a few lytic cells (Figure 4.10). These results suggest that deletion of gene x blocks the apoptotic pathway in GL261 cells more effectively than in CT2A cells.

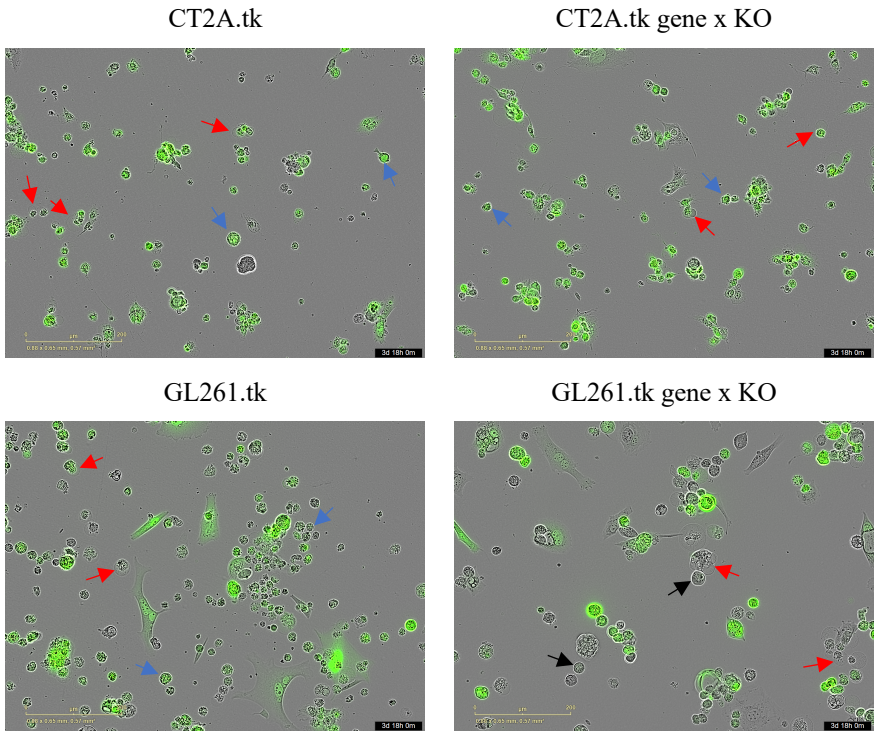

Figure 4.10: Differences in morphological features at 3 days 18 hours following 20 µM GCV treatment. Following HSV-TK/GCV SGT, a representative image for each cell line (CT2A.tk, CT2A.tk gene x KO, GL261.tk and GL261.tk gene x KO) was extracted at 3 days 18 hours following GCV treatment. Arrows indicate apoptotic (blue), lytic (red) and smooth round cells (black). Real time cell morphological changes were captured using Incucyte® S3 system at ×20 objective. Scale bar: 200 µm. Better quality images can be accessed here: https://1drv.ms/f/s!Aj2lWAkKR6YU0RwGNSbjgqvQXrTS?e=jQckiL

Reduced executioner caspases (3 and 7) activity and visual detection of lytic cell death in the KO cells prompted us to quantify the extent of lytic cell death in all cell lines. Quantification of cells exhibiting lytic cell death morphology (shown in Figure 4.9) was performed. A significantly higher count was observed in CT2A.tk relative to CT2A.tk gene x KO whereas the differences between GL261.tk and GL261.tk gene x KO were minimal (Figure 4.11).

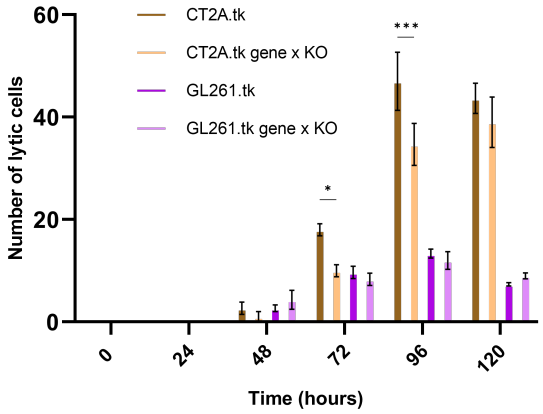

Figure 4.11: Quantification of pyroptotic morphology exhibiting cells. An equal number of cells for all cell lines was treated with 20 µM GCV. A manual count of cells exhibiting bubble-like protrusions suggestive of lytic cell death was performed on 3 replicate images (for each cell line) captured using Incucyte® S3 system at 20× objective. Statistics were performed by Two-way ANOVA followed by Tukey's multiple comparisons test, * , $p < 0.05$, ** , $p < 0.01$ and ****, $p < 0.0001$. Non-significant comparisons not shown. The graphs and error bars were plotted with mean and SEM.

4.6 Potential activation of non-apoptotic cell-death mechanism in the gene x KO cells following HSV-TK/GCV SGT

To further identify the nature of the acquired mechanism of cell death due to the deletion of gene x, further investigations were conducted. In this process, we employed PI uptake assay which serves as a marker for immunoinflammatory and lytic type of cell death [110, 111]. For the PI uptake assay, gene x KO cells were subjected to HSV-TK/GCV SGT and thereafter, the PI uptake was measured at various time points using the Incucyte® S3 system.

GCV treated CT2A.tk and CT2A.tk gene x KO cells showed comparable, steady rises in PI uptake from the time of GCV treatment throughout to 120 hours. Untreated cells on the other hand, showed a slight rise from 0 to 24 hours followed by a steady drop (Figure 4.12a). On the other hand, while GL261.tk gene x KO cells showed a rise in PI uptake from the time of GCV treatment throughout to 120 hours, a distinctly higher PI uptake was seen in GL261.tk relative to GL261.tk gene x KO at 96 hours. That was however followed by a drop in PI uptake at 120 hours (Figure 4.12b). These results show no indication of increased lytic cell death in gene x KO cells.

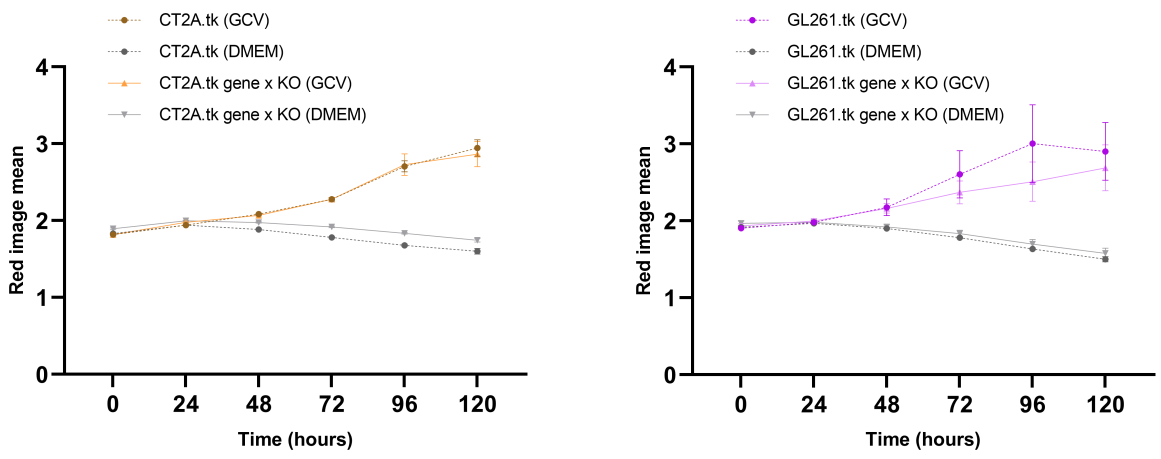

(a) (b)

Figure 4.12: Quantification of gene x KO cells PI uptake following HST-TK/GCV SGT. An equal number of CT2A.tk, CT2A.tk gene x KO (a), GL261.tk and GL261.tk gene x KO (b) cells was seeded followed by overnight incubation at 37°C after which, cells were either left untreated in PI supplemented media (DMEM) or treated with 20 µM GCV in PI supplemented media (GCV) for indicated times. Two well replicates were included for each cell line with 9 images per well taken using Incucyte® S3 system at 20× objective. The red image mean, (indicative of PI uptake) was calculated for each cell line using Incucyte® S3 software. Statistics were performed by Two-way ANOVA followed by Tukey's multiple comparisons test, * , $p < 0.05$, ** , $p < 0.01$ and ****, $p < 0.0001$. Non-significant comparisons not shown. The graphs and error bars were plotted with mean and SEM.

Chapter 5

5 Discussion

The efficacy of SGT in the treatment of GBM has been extensively studied [112-114]. Implementation of SGT in animal models and small-scale clinical trials has yielded promising results [112, 115, 116]. However, similar results in large-scale trials could not be replicated [53], which in turn warranted for further developments of SGT by targeting various aspects of SGT (such as choice of vector, suicide gene and prodrug) and prompted development of more research work targeting the in-depth understanding of GBM biology (cell death included) [117-119]. In this work, we subjected CT2A and GL261, the two most common murine glioma models, to HSV-TK/GCV SGT following KO of two critical genes involved in the intrinsic apoptotic pathway through CRISPR/Cas9 technology.

In a previous study from our lab, CT2A and GL261 cells were subjected to HSV-TK/GCV SGT, after which the mode of cell death was studied. Results demonstrated activation of the apoptotic pathway as suggested by cytochrome c release and cleavage of caspase-9. The induction of apoptotic cell death observed in this study is consistent with results obtained from previous studies involving human glioma cell lines LN-18, LN-229 and U87 in which HSV-TK/GCV SGT similarly induced apoptotic cell death [50, 96]. The knowledge that apoptosis is regarded as a non-immunogenic cell death [93], prompted us to investigate if – blocking the intrinsic apoptotic pathway can reroute the cell death mechanism into a lytic type of cell death that could potentially improve the efficacy of HSV-TK/GCV SGT. Over the last few years, the necessity of an active anti-tumor immune response has been highly appreciated in order to achieve an effective treatment response. Lytic cell death mechanisms, unlike apoptosis, owing to the rupture of cell membrane allow release of cellular materials which could act as pro-inflammatory molecules or neo-antigens. This, in turn, may ignite an anti-tumor immune response in addition to the known tumor cell-killing by SGT. To investigate if the SGT-mediated cell death mechanism can be rendered into a lytic, inflammatory type of cell death, we genetically modified two murine glioma cell models (CT2A and GL261). We knocked out two key genes involved in the relevant apoptotic pathway (gene x

and y). Upon verification of gene x KO and obtaining successful results, we decided to pursue only gene x studies due to limited time.

5.1 CRISPR Cas9 technology facilitates KO of our gene of interest

Raptinal is known to induce cytotoxicity in cancer cells by triggering cytochrome c release, thereby activating the intrinsic apoptotic pathway and, by simultaneously shutting down the mitochondrial function, thereby exerting caspase-independent cytotoxic effects [120]. Because of this and raptinal also being a rapid inducer of apoptosis, we used raptinal treatment as a tool to isolate the clones with complete knock-out of our gene of interest from both cell models. Immunoblotting results revealed a clear reduction of full-length gene x and lack of cleaved product of gene x following raptinal treatment in the KO cells of each cell. Furthermore, WST results demonstrated a delay in cell death of the KO cells compared to wt cells. Taken together, these observations implied efficient KO of our gene of interest in the selected clones CT2A and GL261 cells.

5.2 Deletion of gene x interferes HSV-TK/GCV SGT-mediated cytotoxicity in CT2A and GL261

Incucyte® S3 system images showing morphological changes occurring post GCV treatment revealed a delay in CT2A.tk gene x KO and GL261.tk gene x KO cell death as compared to CTA.tk and GL261.tk, respectively (Figure 4.9). This was confirmed by WST assay. A statistically significant difference in cell viability between the KO cells and their wt counterpart was detected only at 48 hours in both cell lines. A reason for this could be that replicates included in the experiment (4) were not enough to reach statistical significance at other time points which showed a similar trend in viability difference. Our data of delayed cell death by knocking out gene X are a unique observation and similar findings have not been reported yet for HSV-TK/GCV SGT treatment. A study previously conducted on mice revealed a link between mutated caspase-9 gene and decreased apoptosis [121].

With the knowledge of apoptotic pathway activation following HSV.TK/GCV SGT previously observed by our lab (unpublished data), the delay in cell death by knocking out gene X was expected as it is crucial in the activation of the apoptotic pathway. Taken together our results

suggested that absence of gene x delays HSV-TK/GCV SGT-mediated cytotoxicity in CT2A and GL261cells. This result prompted us to further investigate the apoptotic pathway in CT2A.tk gene x KO and GL261.tk gene x KO after GCV treatment

Immunoblot analysis revealed less caspase-3 activation in CT2A.tk gene x KO and GL261.tk gene x KO relative to CT2A.tk and GL261.tk, respectively. This observation was not surprising as it is already known that active caspase-9 facilitates caspase-3 and -7 activation during apoptosis [76, 122]. Other studies have demonstrated overlapping but also distinct roles of caspase-3 and -7 in apoptosis [123, 124] and the importance of caspase-3 and -7 in apoptosis seems to be dependent upon cell type and apoptotic stimuli [125]. In another study activated caspase-3 was dominant and necessary for efficient cell killing, whereas no major role for activated caspase-7 in intrinsic cell death could be demonstrated [123]. To rule out the involvement of caspase-7-mediated apoptosis, cleavage of caspase-7 was also investigated. A very low accumulation of activated caspase-7 was detected in all cell lines at all time points, with minimal detection in CT2A.tk and GL26.tk at 48- and 72-hour time points. Overall, our results indicate that intrinsic apoptosis was no longer the dominant mode of cell death in the gene x KO cells. To further confirm this statement, we checked the cleavage of PARP-1, which is a substrate for both activated caspase-3 and -7 [126].

PARP-1 is responsible for detection and repair of DNA damage [127]. Severely DNA damaged cells demonstrate amplified PARP-1 activity which causes depletion of cell's ATP pools [128]. If unchecked, prolonged ATP depletion will lead to passive necrotic cell death [129]. To avoid this during apoptosis, activated caspase-3 facilitates cleavage and inactivation of PARP-1. Failure of PARP-1 cleavage by caspases results in necrotic induction and enhanced apoptosis [129].
Based on this knowledge, we investigated PARP-1 cleavage in CT2A.tk gene x KO and GL261.tk gene x KO. PARP-1 cleavage was clearly detected in CT2A.tk and GL261.tk following GCV treatment, with decreasing expression as time elapsed. Complimentary to this, caspase-3 activation increased from 48 to 72 hours and thereafter remained constantly high at 96 hours. This result indicated the enhancement of apoptosis in response to a high PARP-1 cleavage at 48 hours.
In CT2A.tk gene x KO, reduced caspase-3 cleavage and minimal PARP-1 cleavage, compared to tk cells, was observed under SGT. In GL261.tk gene x KO cells, PARP-1 cleavage was absent, and caspase-3 cleavage substantially reduced compared to GL261.tk cells. These results further

confirm that the classical apoptotic pathway is no longer the dominant mode of cell death in the gene x KO cells following SGT. Furthermore, the effects were more pronounced in GL261 than CT2A. Previous and pioneering studies on caspase-9 knockout in mice demonstrated failure of caspase-3 activation and reduced apoptosis, which is a similar result [121, 130].

Besides apoptosis, cells can undergo other types of cell death dependent on the molecular machinery and circumstances [128, 131]. Thus, we proceeded to investigate possible activation of lytic pathways in CT2A.tk gene x KO.tk and GL261.tk gene x KO.

5.3 Lack of evidence of increased lytic cell death in the KO cells

During analysis of videos, apoptotic morphological changes were seen in CT2A.tk and GL261.tk. This included shrinkage of the cells, plasma membrane blebbing, and nuclear condensation. These features are amongst the known hallmarks of apoptosis [132]. The same was observed for CT2A.tk gene x KO cells, but not for GL261.tk gene x KO cells to a similar extent. The latter showed cell rounding, but no shrinkage or cell blebbing. After 48 hours and at later time points, all tk and tk gene x KO cells showed so-called bubble formation which corresponds to release of cell contents and thus to a lytic/necrotic type of cell death. It is known that apoptotic cells undergo secondary necrosis in vitro [133, 134]. Under normal conditions, this is not observed in vivo as macrophages are attracted by apoptotic cells and phagocytosed [135]. Thus, for apoptotic cells, the lysis is secondary and not the immediate cell death mechanism.

One interesting observation from our results is that GL261.tk gene x KO cells undergo a lytic/necrotic type of cell death without preceding apoptosis (as suggested by absence of apoptotic cell morphology in the videos, low caspase-3 activation and absence of PARP-1 cleavage). This result may indicate a primary necrotic/lytic cell death. Quantification of lytic cell morphology did not reveal any significant increase in lytic cell death between GL261.tk and GL261.tk gene x KO. However, quantification of lytic morphology is prone to human error and to confirm this result we further employed PI uptake assay which again showed an insignificant difference in PI uptake between GL261.tk and GL261.tk gene x KO. Although there was no difference in the amount of lytic cell death between GL261.tk and GL261.tk gene x KO, the nearly complete absence of

apoptosis in GL261.tk gene x KO at the morphological and molecular level, indicates a different mode of cell death which may be of primary or secondary necrotic/lytic nature

There have been two major types of necrotic cell death discovered in the last decade named pyroptosis and necroptosis. Pyroptosis is mediated by the family of Gasdermin proteins [136]. Interestingly, Gasdermin E (GSDME) has been demonstrated to switch caspase-3 mediated apoptosis induced by chemotherapy drugs to pyroptosis in certain cancer cells expressing GSDME. Specifically, the cleavage of GSDME by activated caspase-3 causes pyroptosis [137].

In a study conducted by Zhang et. al, their findings revealed that the level of GSDME expressed by caspase-3 activated cells determine the form of cell death they undergo [137]. Furthermore, they showed that cells with high GSDME expression undergo pyroptosis following their stimulation by an apoptotic stimulating agent such as chemotherapeutic drugs. On the other hand, cells with low GSDME expression undergo apoptosis which can develop into secondary necrosis [137]. However, it is important to note that this study was not conducted in GBM cell lines. While most cancer cells have low GSDME expression, GSDME expression has been seen to be high in GBM patients' cells [138]. Simultaneous activation of apoptosis and pyroptosis in GBM is not a new phenomenon as this has been seen in various studies [131, 139, 140]. However, in our experiments, Caspase-3 activation is heavily reduced in tk gene x KO cells which makes activation of GSDME unlikely.

Necroptosis is another mode of lytic cell death and is activated through the tumor necrosis factor receptor (TNFR) pathway [141]. Necroptosis is presumed to be the alternative tumor cell death pathway activated in GBM cells following inhibition of apoptosis [142]. It has been reported that elimination of post-mitochondrial apoptotic signals such as caspase activation may switch apoptosis to necrosis [143]. While some *in vitro* studies have shown that necroptosis induction through drugs can inhibit glioma proliferation [144, 145], Sicheng Wan et.al., identified an association between necroptosis activation and poor glioma patients prognosis [146]. This signifies the need for further research on necroptosis significance in glioma cell death which also concerns our study.

5.4 Conclusions and future perspectives

Our findings in this study indicate that deletion of gene x has a heterogenous response to HSV-TK/GCV SGT induced apoptotic cell death in CT2A and GL261 glioma cell lines. While CT2A KO cells showed a delay in apoptotic response, in GL261 KO cells no evidence could support induction of apoptosis. Morphological signs of apoptosis were not seen in addition to absence of PARP-1 cleavage by western blot. In both cell models, intrinsic pathway of apoptosis was not a major cell death mode, and this is more pronounced in GL261 than CT2A. The most interesting results of this work, which need to be explored in the future are (i) the activated mode of cell death in GL261.tk gene x KO cells and (ii) induction of lytic cell death in GL261 KO cells without preceding apoptosis.

Research studies have already shown that involvement of the hosts' immune response may be the pathway leading to the achievement of successful HSV-TK/GCV gene therapy targeting cancer cells [147]. Discovery of therapeutic strategies that induce lytic cell death mechanisms such as pyroptosis or necroptosis may offer solutions towards this pursuit. This is especially possible in GBM considering its high expression of GSDME (a crucial protein in pyroptosis cell death induction).

We could not conduct further investigations on CT2A and GL261-gene y KO cells due to the time limit. Therefore, pursuit of these investigations is highly recommended in the future to confirm our results with gene X. In our study, further investigations also need to be conducted to explore the mechanism involved in the activation of caspase-3 in CT2A.tk gene x KO and GL261.tk gene x KO in the absence of gene x. Considering that apoptosis involves the intrinsic and extrinsic pathway, further investigations exploring possible induction of the extrinsic pathway following deletion of gene x, (by investigating caspase-8 activation) as an escape route may be worth analyzing. This would be even more recommended in CT2A KO cells due to the observed weak caspase-3 activation and PARP-1 cleavage which is more pronounced in CT2A than GL261 KO cells. Considering the very high morphological similarities exhibited by apoptotic and pyroptotic cells, in addition to the expression of activated caspase-3 in both modes of cell death, determination of GSDME cleavage may be effective in distinguishing between pyroptotic and apoptotic cell death mechanisms.

To curb for false positive PI uptake results that can be obtained in late-stage apoptotic cells, the modified annexin V/ propidium iodide apoptotic assay designed by Aja M et al [148] could be utilized as it minimizes false positive results. Lactate dehydrogenase (LDH) assay can also be performed as a complementary test to PI uptake assay. Clear induction of lytic cell death was apparent in both cell lines. And apoptosis was clearly reduced to a substantial extent. Thus, it is very likely that other kinds of cell death mechanisms may occur. Glioma cells are known to be prone to autophagy [149]. Further investigations should be done to assess possible induction of autophagic cell death. This can be done by investigating the expression of p62/Sequestosome 1 (SQSTM1) and detecting the conversion of microtubule-associated protein 1A/1B-light chain 3 (MAP1LC3), (frequently referred to as LC3) from LC3-I to LC3-II as these features accompany autophagic cell death [150]. Immunoblotting techniques can be utilized for this purpose.

Should the cells undergo autophagy, it would still be interesting to pursue further studies to see if the rerouting of cell death mechanism can affect the tumor immune microenvironment. Although autophagic cell death is fundamentally different from pyroptosis and necroptosis, the effect of autophagic cell death in the tumor microenvironment and the tumor immunomicroenvironment is highly context dependent.

References

1. Diori Karidio, I. and S.H. Sanlier, *Reviewing cancer's biology: an eclectic approach*. 2021. p. 32.
2. Hausman, D.M., *What Is Cancer?* 2019: Baltimore, Md. :. p. 778-784.
3. Bray, F., et al., *Global cancer statistics 2018: GLOBOCAN estimates of incidence and mortality worldwide for 36 cancers in 185 countries*. 2018: New York :. p. 394-424.
4. Sung, H., et al., *Global Cancer Statistics 2020: GLOBOCAN Estimates of Incidence and Mortality Worldwide for 36 Cancers in 185 Countries*. 2021: New York :. p. 209-249.
5. Prior, I.A., F.E. Hood, and J.L. Hartley, *The Frequency of Ras Mutations in Cancer*. 2020: Philadelphia, Pa. p. 2969-2974.
6. Annibali, D., et al., *Myc inhibition is effective against glioma and reveals a role for Myc in proficient mitosis*. 2014: [London] :. p. 4632.
7. Hutter, S., et al., *Modeling and Targeting MYC Genes in Childhood Brain Tumors.* Genes (Basel), 2017. **8**(4).
8. Davies, H., et al., *Mutations of the BRAF gene in human cancer*. 2002: [London] :. p. 949-954.
9. Vogelstein, B. and K.W. Kinzler, *Cancer genes and the pathways they control*. 2004: New York, N.Y. :. p. 789-799.
10. Hong, B., et al., *Targeting tumor suppressor p53 for cancer therapy: strategies, challenges and opportunities*. 2014. p. 80-89.
11. Dyson, N.J., *RB1: a prototype tumor suppressor and an enigma*. 2016: [Cold Spring Harbor, N.Y.] :. p. 1492-1502.
12. Tung, N., et al., *Frequency of mutations in individuals with breast cancer referred for BRCA1 and BRCA2 testing using next-generation sequencing with a 25-gene panel*. 2015: [New York, NY] :. p. 25-33.
13. Nowell, P.C., *Tumor progression: a brief historical perspective*. 2002: London :. p. 261-266.
14. Cai, Q. and Z. Yuan, *Overview of Infectious Causes of Human Cancers*. 2017: New York. p. 1-9.
15. De Flora, S. and S. La Maestra, *Epidemiology of cancers of infectious origin and prevention strategies*. 2015: Pisa, Italy :. p. E15-E20.
16. Liu, H. and Z. Dong, *Cancer Etiology and Prevention Principle: "1 + X"*. 2021: Philadelphia, Pa. p. 5377-5395.
17. Hanahan, D. and R.A. Weinberg, *The hallmarks of cancer*. 2000: Cambridge, Mass. :. p. 57-70.
18. Hanahan, D. and R.A. Weinberg, *Hallmarks of cancer: the next generation.* Cell, 2011. **144**(5): p. 646-74.
19. Hanahan, D., *Hallmarks of Cancer: New Dimensions*. 2022: Philadelphia, PA :. p. 31-46.
20. McFaline-Figueroa, J.R. and E.Q. Lee, *Brain Tumors*. 2018: [New York, NY] :. p. 874-882.
21. Nayak, L., E.Q. Lee, and P.Y. Wen, *Epidemiology of brain metastases*. 2012: [Philadelphia, Pa.] :. p. 48-54.
22. Arvold, N.D., et al., *Updates in the management of brain metastases*. 2016: Charlottesville, VA :. p. 1043-1065.

23. Lutterbach, J., S. Bartelt, and C. Ostertag, *Long-term survival in patients with brain metastases*. 2002: Heidelberg :. p. 417-425.
24. Louis, D.N., et al., *The 2016 World Health Organization Classification of Tumors of the Central Nervous System: a summary*. 2016: Heidelberg :. p. 803-820.
25. Ostrom, Q.T., et al., *CBTRUS Statistical Report: Primary Brain and Central Nervous System Tumors Diagnosed in the United States in 2008-2012*. 2015: Charlottesville, VA :. p. iv1-iv62.
26. Ostrom, Q.T., et al., *CBTRUS Statistical Report: Primary Brain and Other Central Nervous System Tumors Diagnosed in the United States in 2014-2018*. 2021: Charlottesville, VA :. p. iii1-iii105.
27. Miller, K.D., et al., *Brain and other central nervous system tumor statistics, 2021.* CA Cancer J Clin, 2021. **71**(5): p. 381-406.
28. Louis, D.N., et al., *The 2021 WHO Classification of Tumors of the Central Nervous System: a summary*. 2021: Charlottesville, VA :. p. 1231-1251.
29. Ohgaki, H. and P. Kleihues, *The definition of primary and secondary glioblastoma*. 2013: [S.l.]. p. 764-772.
30. Verhaak, R.G., et al., *Integrated genomic analysis identifies clinically relevant subtypes of glioblastoma characterized by abnormalities in PDGFRA, IDH1, EGFR, and NF1.* Cancer Cell, 2010. **17**(1): p. 98-110.
31. Sidaway, P., *CNS cancer: Glioblastoma subtypes revisited.* Nat Rev Clin Oncol, 2017. **14**(10): p. 587.
32. Sottoriva, A., et al., *Intratumor heterogeneity in human glioblastoma reflects cancer evolutionary dynamics.* Proc Natl Acad Sci U S A, 2013. **110**(10): p. 4009-14.
33. Patel, A.P., et al., *Single-cell RNA-seq highlights intratumoral heterogeneity in primary glioblastoma*. 2014: Washington, D.C. p. 1396-1401.
34. Lapointe, S., A. Perry, and N.A. Butowski, *Primary brain tumours in adults*. 2018: London. p. 432-446.
35. Stupp, R., et al., *Radiotherapy plus concomitant and adjuvant temozolomide for glioblastoma*. 2005: Boston, MA :. p. 987-996.
36. Li, Y., et al., *Bevacizumab in Recurrent Glioma: Patterns of Treatment Failure and Implications*. 2017: Goyang, Republic of Korea :. p. 1-9.
37. Gramatzki, D., et al., *Bevacizumab may improve quality of life, but not overall survival in glioblastoma: an epidemiological study*. 2018: [Dordrecht] :. p. 1431-1436.
38. Thakur, A., et al., *Glioblastoma: Current Status, Emerging Targets, and Recent Advances*. 2022: Washington, D.C. p. 8596-8685.
39. Kang, J.H. and A. Desjardins, *Convection-enhanced delivery for high-grade glioma*. 2022: Oxford :. p. 24-34.
40. Norden, A.D., et al., *An exploratory survival analysis of anti-angiogenic therapy for recurrent malignant glioma*. 2009: [Dordrecht] :. p. 149-155.
41. Chen, Z. and D. Hambardzumyan, *Immune Microenvironment in Glioblastoma Subtypes.* Front Immunol, 2018. **9**: p. 1004.
42. Charles, N.A., et al., *The brain tumor microenvironment.* Glia, 2012. **60**(3): p. 502-14.
43. Hambardzumyan, D., D.H. Gutmann, and H. Kettenmann, *The role of microglia and macrophages in glioma maintenance and progression.* Nat Neurosci, 2016. **19**(1): p. 20-7.
44. Reardon, D.A., et al., *Effect of Nivolumab vs Bevacizumab in Patients With Recurrent Glioblastoma: The CheckMate 143 Phase 3 Randomized Clinical Trial.* JAMA Oncol, 2020. **6**(7): p. 1003-1010.

45. Yang, T., Z. Kong, and W. Ma, *PD-1/PD-L1 immune checkpoint inhibitors in glioblastoma: clinical studies, challenges and potential.* Hum Vaccin Immunother, 2021. **17**(2): p. 546-553.
46. Stupp, R., et al., *Effect of Tumor-Treating Fields Plus Maintenance Temozolomide vs Maintenance Temozolomide Alone on Survival in Patients With Glioblastoma: A Randomized Clinical Trial.* JAMA, 2017. **318**(23): p. 2306-2316.
47. Niedba?a, M., et al., *Glioblastoma: Pitfalls and Opportunities of Immunotherapeutic Combinations*. 2022: [Auckland, N.Z.] :. p. 437-468.
48. Juratli, T.A., G. Schackert, and D. Krex, *Current status of local therapy in malignant gliomas--a clinical review of three selected approaches*. 2013: [Oxford] :. p. 341-358.
49. Dent, P., et al., *Searching for a cure: gene therapy for glioblastoma*. 2008: Georgetown, TX :. p. 1335-1340.
50. Fischer, U., et al., *Mechanisms of thymidine kinase/ganciclovir and cytosine deaminase/ 5-fluorocytosine suicide gene therapy-induced cell death in glioma cells.* Oncogene, 2005. **24**(7): p. 1231-43.
51. Moolten, F.L., *Tumor chemosensitivity conferred by inserted herpes thymidine kinase genes: paradigm for a prospective cancer control strategy.* Cancer Res, 1986. **46**(10): p. 5276-81.
52. Brewster, M.E., et al., *Enhanced delivery of ganciclovir to the brain through the use of redox targeting*. 1994: Washington, DC. p. 817-823.
53. Rainov, N.G., *A phase III clinical evaluation of herpes simplex virus type 1 thymidine kinase and ganciclovir gene therapy as an adjuvant to surgical resection and radiation in adults with previously untreated glioblastoma multiforme.* Hum Gene Ther, 2000. **11**(17): p. 2389-401.
54. Okura, H., C.A. Smith, and J.T. Rutka, *Gene therapy for malignant glioma*. 2014: London :. p. 21.
55. Kane, J.R., et al., *Sui generis: gene therapy and delivery systems for the treatment of glioblastoma*. 2015: Charlottesville, VA :. p. ii24-ii36.
56. Rainov, N.G. and V. Heidecke, *Clinical development of experimental therapies for malignant glioma.* Sultan Qaboos Univ Med J, 2011. **11**(1): p. 5-28.
57. Huszthy, P.C., et al., *Remission of invasive, cancer stem-like glioblastoma xenografts using lentiviral vector-mediated suicide gene therapy.* PLoS One, 2009. **4**(7): p. e6314.
58. Gatson, N.N., E.A. Chiocca, and B. Kaur, *Anti-angiogenic gene therapy in the treatment of malignant gliomas.* Neurosci Lett, 2012. **527**(2): p. 62-70.
59. Hossain, J.A., et al., *Lentiviral HSV-Tk.007-mediated suicide gene therapy is not toxic for normal brain cells.* J Gene Med, 2016. **18**(9): p. 234-43.
60. Cotter, T.G., *Apoptosis and cancer: the genesis of a research field*. 2009: England :. p. 501-507.
61. Green, D.R., et al., *Immunogenic and tolerogenic cell death.* Nat Rev Immunol, 2009. **9**(5): p. 353-63.
62. Hengartner, M.O., *The biochemistry of apoptosis*. 2000: [London] :. p. 770-776.
63. Kerr, J.F., C.M. Winterford, and B.V. Harmon, *Apoptosis. Its significance in cancer and cancer therapy*. 1994: [New York, NY] :. p. 2013-2026.
64. Fulda, S. and K.M. Debatin, *Apoptosis signaling in tumor therapy.* Ann N Y Acad Sci, 2004. **1028**: p. 150-6.

65. Kashyap, D., V.K. Garg, and N. Goel, *Intrinsic and extrinsic pathways of apoptosis: Role in cancer development and prognosis.* Adv Protein Chem Struct Biol, 2021. **125**: p. 73-120.
66. Loreto, C., et al., *The role of intrinsic pathway in apoptosis activation and progression in Peyronie's disease.* Biomed Res Int, 2014. **2014**: p. 616149.
67. Taylor, R.C., S.P. Cullen, and S.J. Martin, *Apoptosis: controlled demolition at the cellular level.* Nat Rev Mol Cell Biol, 2008. **9**(3): p. 231-41.
68. Degterev, A., M. Boyce, and J. Yuan, *A decade of caspases.* Oncogene, 2003. **22**(53): p. 8543-67.
69. Earnshaw, W.C., L.M. Martins, and S.H. Kaufmann, *Mammalian caspases: structure, activation, substrates, and functions during apoptosis.* Annu Rev Biochem, 1999. **68**: p. 383-424.
70. Alberts, B., J.H. Wilson, and T. Hunt, *Molecular Biology of the Cell*. 6th ed. 2015, New York: Garland Science :. p.1023.
71. Ashkenazi, A., *Targeting the extrinsic apoptotic pathway in cancer: lessons learned and future directions.* J Clin Invest, 2015. **125**(2): p. 487-9.
72. Fulda, S., *Cell death-based treatment of glioblastoma*. 2018: [New York] :. p. 121.
73. Fulda, S., L. Galluzzi, and G. Kroemer, *Targeting mitochondria for cancer therapy.* Nat Rev Drug Discov, 2010. **9**(6): p. 447-64.
74. Cain, K., *Chemical-induced apoptosis: formation of the Apaf-1 apoptosome.* Drug Metab Rev, 2003. **35**(4): p. 337-63.
75. Rodriguez, J. and Y. Lazebnik, *Caspase-9 and APAF-1 form an active holoenzyme.* Genes Dev, 1999. **13**(24): p. 3179-84.
76. Li, P., et al., *Cytochrome c and dATP-dependent formation of Apaf-1/caspase-9 complex initiates an apoptotic protease cascade.* Cell, 1997. **91**(4): p. 479-89.
77. Venereau, E., C. Ceriotti, and M.E. Bianchi, *DAMPs from Cell Death to New Life.* Front Immunol, 2015. **6**: p. 422.
78. Fulda, S. and D. Vucic, *Targeting IAP proteins for therapeutic intervention in cancer.* Nat Rev Drug Discov, 2012. **11**(2): p. 109-24.
79. Fulda, S. and K.M. Debatin, *Extrinsic versus intrinsic apoptosis pathways in anticancer chemotherapy.* Oncogene, 2006. **25**(34): p. 4798-811.
80. Giampazolias, E. and S.W.G. Tait, *Caspase-independent cell death: An anti-cancer double whammy.* Cell Cycle, 2018. **17**(3): p. 269-270.
81. Fulda, S., *Cell death-based treatment of glioblastoma.* Cell Death Dis, 2018. **9**(2): p. 121.
82. Du, C., et al., *Smac, a mitochondrial protein that promotes cytochrome c-dependent caspase activation by eliminating IAP inhibition*. 2000: Cambridge, Mass. :. p. 33-42.
83. Delbridge, A.R.D., et al., *Thirty years of BCL-2: translating cell death discoveries into novel cancer therapies*. 2016: England :. p. 99-109.
84. Jiang, Z., X. Zheng, and K.M. Rich, *Down-regulation of Bcl-2 and Bcl-xL expression with bispecific antisense treatment in glioblastoma cell lines induce cell death.* J Neurochem, 2003. **84**(2): p. 273-81.
85. Liwak, U., et al., *Loss of PDCD4 contributes to enhanced chemoresistance in Glioblastoma multiforme through de-repression of Bcl-xL translation.* Oncotarget, 2013. **4**(9): p. 1365-72.
86. Galluzzi, L., et al., *Consensus guidelines for the definition, detection and interpretation of immunogenic cell death.* J Immunother Cancer, 2020. **8**(1).

87. Moserova, I., et al., *Caspase-2 and oxidative stress underlie the immunogenic potential of high hydrostatic pressure-induced cancer cell death.* Oncoimmunology, 2017. **6**(1): p. e1258505.
88. Verfaillie, T., et al., *Pro-apoptotic signaling induced by photo-oxidative ER stress is amplified by Noxa, not Bim*. 2013: Orlando, Fla. :. p. 500-506.
89. Garg, A.D., et al., *A novel pathway combining calreticulin exposure and ATP secretion in immunogenic cancer cell death.* EMBO J, 2012. **31**(5): p. 1062-79.
90. Decraene, B., et al., *Immunogenic cell death and its therapeutic or prognostic potential in high-grade glioma.* Genes Immun, 2022. **23**(1): p. 1-11.
91. Garg, A.D. and P. Agostinis, *Cell death and immunity in cancer: From danger signals to mimicry of pathogen defense responses.* Immunol Rev, 2017. **280**(1): p. 126-148.
92. Tang, R., et al., *Ferroptosis, necroptosis, and pyroptosis in anticancer immunity.* J Hematol Oncol, 2020. **13**(1): p. 110.
93. Hochreiter-Hufford, A. and K.S. Ravichandran, *Clearing the dead: apoptotic cell sensing, recognition, engulfment, and digestion.* Cold Spring Harb Perspect Biol, 2013. **5**(1): p. a008748.
94. Fucikova, J., et al., *Prognostic and Predictive Value of DAMPs and DAMP-Associated Processes in Cancer.* Front Immunol, 2015. **6**: p. 402.
95. DeCordova, S., et al., *Molecular Heterogeneity and Immunosuppressive Microenvironment in Glioblastoma.* Front Immunol, 2020. **11**: p. 1402.
96. Glaser, T., et al., *Death receptor-independent cytochrome c release and caspase activation mediate thymidine kinase plus ganciclovir-mediated cytotoxicity in LN-18 and LN-229 human malignant glioma cells.* Gene Ther, 2001. **8**(6): p. 469-76.
97. Tomicic, M.T., R. Thust, and B. Kaina, *Ganciclovir-induced apoptosis in HSV-1 thymidine kinase expressing cells: critical role of DNA breaks, Bcl-2 decline and caspase-9 activation.* Oncogene, 2002. **21**(14): p. 2141-53.
98. Brown, J.M. and L.D. Attardi, *The role of apoptosis in cancer development and treatment response.* Nat Rev Cancer, 2005. **5**(3): p. 231-7.
99. Sanjana, N.E., O. Shalem, and F. Zhang, *Improved vectors and genome-wide libraries for CRISPR screening*. 2014: New York :. p. 783-784.
100. Shalem, O., et al., *Genome-scale CRISPR-Cas9 knockout screening in human cells*. 2014: Washington, D.C. p. 84-87.
101. Beckman, G., et al., *G-6-PD and PGM phenotypes of 16 continuous human tumor cell lines. Evidence against cross-contamination and contamination by HeLa cells*. 1971: Basel ; New York :. p. 238-241.
102. Martinez-Murillo, R. and A. Martinez, *Standardization of an orthotopic mouse brain tumor model following transplantation of CT-2A astrocytoma cells.* Histol Histopathol, 2007. **22**(12): p. 1309-26.
103. Pulix, M., et al., *Molecular characterization of HEK293 cells as emerging versatile cell factories*. 2021: [London] :. p. 18-24.
104. Hossain, J.A., et al., *Cancer Suicide Gene Therapy with TK.007*. 2019: Clifton, N.J. :. p. 11-26.
105. Villatoro, A.J., et al., *Suicide gene therapy by canine mesenchymal stem cell transduced with thymidine kinase in a u-87 glioblastoma murine model: Secretory profile and antitumor activity.* PLoS One, 2022. **17**(2): p. e0264001.
106. Schneider, C.A., W.S. Rasband, and K.W. Eliceiri, *NIH Image to ImageJ: 25 years of image analysis.* Nat Methods, 2012. **9**(7): p. 671-5.

107. Crowley, L.C., et al., *Quantitation of Apoptosis and Necrosis by Annexin V Binding, Propidium Iodide Uptake, and Flow Cytometry.* Cold Spring Harb Protoc, 2016. **2016**(11).
108. Palchaudhuri, R., et al., *A Small Molecule that Induces Intrinsic Pathway Apoptosis with Unparalleled Speed.* Cell Rep, 2015. **13**(9): p. 2027-36.
109. Chen, X., et al., *Pyroptosis is driven by non-selective gasdermin-D pore and its morphology is different from MLKL channel-mediated necroptosis.* Cell Res, 2016. **26**(9): p. 1007-20.
110. Fink, S.L. and B.T. Cookson, *Caspase-1-dependent pore formation during pyroptosis leads to osmotic lysis of infected host macrophages.* Cell Microbiol, 2006. **8**(11): p. 1812-25.
111. Yu, P., et al., *Pyroptosis: mechanisms and diseases.* Signal Transduct Target Ther, 2021. **6**(1): p. 128.
112. Tirgar, F., et al., *Preclinical gene therapy in glioblastoma multiforme: Using olfactory ensheathing cells containing a suicide gene.* Life Sci, 2022. **311**(Pt A): p. 121132.
113. Hossain, J.A., et al., *Long-term treatment with valganciclovir improves lentiviral suicide gene therapy of glioblastoma*. 2019: Charlottesville, VA :. p. 890-900.
114. Kim, J., et al., *Poly(ethylene glycol)-Poly(beta-amino ester)-Based Nanoparticles for Suicide Gene Therapy Enhance Brain Penetration and Extend Survival in a Preclinical Human Glioblastoma Orthotopic Xenograft Model.* ACS Biomater Sci Eng, 2020. **6**(5): p. 2943-2955.
115. Ram, Z., et al., *Therapy of malignant brain tumors by intratumoral implantation of retroviral vector-producing cells.* Nat Med, 1997. **3**(12): p. 1354-61.
116. Culver, K.W., et al., *In vivo gene transfer with retroviral vector-producer cells for treatment of experimental brain tumors.* Science, 1992. **256**(5063): p. 1550-2.
117. Hossain, J.A., et al., *Suicide gene therapy for the treatment of high-grade glioma: past lessons, present trends, and future prospects*. [Oxford] :. p. vdaa013.
118. Abbruzzese, C., et al., *Molecular Biology in Glioblastoma Multiforme Treatment.* Cells, 2022. **11**(11).
119. Feng, S., et al., *Immunogenic cell death related risk model to delineate ferroptosis pathway and predict immunotherapy response of patients with GBM.* Front Immunol, 2022. **13**: p. 992855.
120. Heimer, S., et al., *Raptinal bypasses BAX, BAK, and BOK for mitochondrial outer membrane permeabilization and intrinsic apoptosis.* Cell Death Dis, 2019. **10**(8): p. 556.
121. Hakem, R., et al., *Differential requirement for caspase 9 in apoptotic pathways in vivo.* Cell, 1998. **94**(3): p. 339-52.
122. Srinivasula, S.M., et al., *Autoactivation of procaspase-9 by Apaf-1-mediated oligomerization.* Mol Cell, 1998. **1**(7): p. 949-57.
123. Brentnall, M., et al., *Caspase-9, caspase-3 and caspase-7 have distinct roles during intrinsic apoptosis.* BMC Cell Biol, 2013. **14**: p. 32.
124. Lakhani, S.A., et al., *Caspases 3 and 7: key mediators of mitochondrial events of apoptosis.* Science, 2006. **311**(5762): p. 847-51.
125. Lamkanfi, M. and T.D. Kanneganti, *Caspase-7: a protease involved in apoptosis and inflammation.* Int J Biochem Cell Biol, 2010. **42**(1): p. 21-4.
126. Chaitanya, G.V., A.J. Steven, and P.P. Babu, *PARP-1 cleavage fragments: signatures of cell-death proteases in neurodegeneration.* Cell Commun Signal, 2010. **8**: p. 31.

127. Boulares, A.H., et al., *Role of poly(ADP-ribose) polymerase (PARP) cleavage in apoptosis. Caspase 3-resistant PARP mutant increases rates of apoptosis in transfected cells.* J Biol Chem, 1999. **274**(33): p. 22932-40.
128. Eguchi, Y., S. Shimizu, and Y. Tsujimoto, *Intracellular ATP levels determine cell death fate by apoptosis or necrosis.* Cancer Res, 1997. **57**(10): p. 1835-40.
129. Herceg, Z. and Z.Q. Wang, *Failure of poly(ADP-ribose) polymerase cleavage by caspases leads to induction of necrosis and enhanced apoptosis.* Mol Cell Biol, 1999. **19**(7): p. 5124-33.
130. Kuida, K., et al., *Reduced apoptosis and cytochrome c-mediated caspase activation in mice lacking caspase 9.* Cell, 1998. **94**(3): p. 325-37.
131. Ren, L.W., et al., *Benzimidazoles induce concurrent apoptosis and pyroptosis of human glioblastoma cells via arresting cell cycle.* Acta Pharmacol Sin, 2022. **43**(1): p. 194-208.
132. Saraste, A. and K. Pulkki, *Morphologic and biochemical hallmarks of apoptosis.* Cardiovasc Res, 2000. **45**(3): p. 528-37.
133. Don, M.M., et al., *Death of cells by apoptosis following attachment of specifically allergized lymphocytes in vitro.* Aust J Exp Biol Med Sci, 1977. **55**(4): p. 407-17.
134. Silva, M.T., A. do Vale, and N.M. dos Santos, *Secondary necrosis in multicellular animals: an outcome of apoptosis with pathogenic implications.* Apoptosis, 2008. **13**(4): p. 463-82.
135. deCathelineau, A.M. and P.M. Henson, *The final step in programmed cell death: phagocytes carry apoptotic cells to the grave.* Essays Biochem, 2003. **39**: p. 105-17.
136. Shi, J., W. Gao, and F. Shao, *Pyroptosis: Gasdermin-Mediated Programmed Necrotic Cell Death.* Trends Biochem Sci, 2017. **42**(4): p. 245-254.
137. Zhang, X. and H. Zhang, *Chemotherapy drugs induce pyroptosis through caspase-3-dependent cleavage of GSDME.* Sci China Life Sci, 2018. **61**(6): p. 739-740.
138. Wan, S., et al., *Pyroptosis, ferroptosis, and autophagy cross-talk in glioblastoma opens up new avenues for glioblastoma treatment.* Cell Commun Signal, 2023. **21**(1): p. 115.
139. Zhao, W., et al., *The CDK inhibitor AT7519 inhibits human glioblastoma cell growth by inducing apoptosis, pyroptosis and cell cycle arrest.* Cell Death Dis, 2023. **14**(1): p. 11.
140. Li, W., et al., *4,5-Dimethoxycanthin-6-one is a novel LSD1 inhibitor that inhibits proliferation of glioblastoma cells and induces apoptosis and pyroptosis.* Cancer Cell Int, 2022. **22**(1): p. 32.
141. Laster, S.M., J.G. Wood, and L.R. Gooding, *Tumor necrosis factor can induce both apoptic and necrotic forms of cell lysis.* J Immunol, 1988. **141**(8): p. 2629-34.
142. Jiang, Y.G., Y. Peng, and K.S. Koussougbo, *Necroptosis: a novel therapeutic target for glioblastoma.* Med Hypotheses, 2011. **76**(3): p. 350-2.
143. Nicotera, P. and G. Melino, *Regulation of the apoptosis-necrosis switch.* Oncogene, 2004. **23**(16): p. 2757-65.
144. Zhou, J., et al., *Emodin induced necroptosis in the glioma cell line U251 via the TNF-alpha/RIP1/RIP3 pathway.* Invest New Drugs, 2020. **38**(1): p. 50-59.
145. Pagano, C., et al., *N6-isopentenyladenosine induces cell death through necroptosis in human glioblastoma cells.* Cell Death Discov, 2022. **8**(1): p. 173.
146. Wan, S., et al., *Combined bulk RNA-seq and single-cell RNA-seq identifies a necroptosis-related prognostic signature associated with inhibitory immune microenvironment in glioma.* Front Immunol, 2022. **13**: p. 1013094.

147. Kuriyama, S., et al., *Cancer gene therapy with HSV-tk/GCV system depends on T-cell-mediated immune responses and causes apoptotic death of tumor cells in vivo.* Int J Cancer, 1999. **83**(3): p. 374-80.
148. Rieger, A.M., et al., *Modified annexin V/propidium iodide apoptosis assay for accurate assessment of cell death.* J Vis Exp, 2011(50).
149. Buccarelli, M., et al., *Inhibition of autophagy increases susceptibility of glioblastoma stem cells to temozolomide by igniting ferroptosis.* Cell Death Dis, 2018. **9**(8): p. 841.
150. Niklaus, M., et al., *Expression analysis of LC3B and p62 indicates intact activated autophagy is associated with an unfavorable prognosis in colon cancer.* Oncotarget, 2017. **8**(33): p. 54604-54615.